

FISBe: A real-world benchmark dataset for instance segmentation of long-range thin filamentous structures

Lisa Mais^{1,2,4,*}, Peter Hirsch^{1,2,*}, Claire Managan³, Ramya Kandarpa³,
 Josef Lorenz Rumberger^{1,2}, Annika Reinke^{2,5}, Lena Maier-Hein^{2,5},
 Gudrun Ihrke³, Dagmar Kainmueller^{1,2,4}

¹ Max-Delbrueck-Center for Molecular Medicine in the Helmholtz Association (MDC) ² Helmholtz Imaging

³ HHMI Janelia Research Campus ⁴ University of Potsdam ⁵ German Cancer Research Center (DKFZ)

✉ {firstname.lastname}@mdc-berlin.de * shared first authors

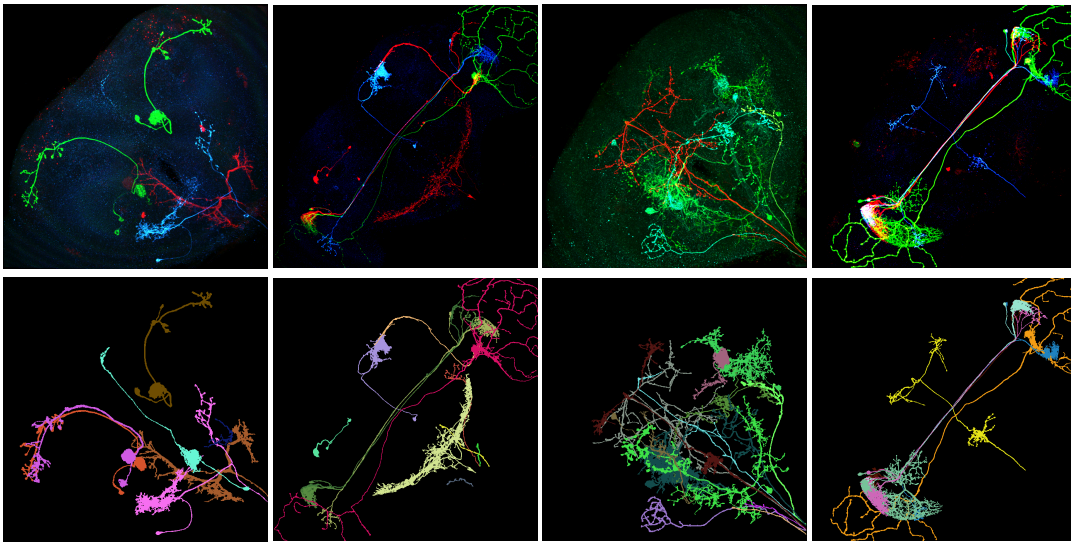


Figure 1. We release the FlyLight Instance Segmentation Benchmark (FISBe) dataset, a 3d multi-color light microscopy dataset of neuronal morphologies in the brain of the fruit fly *Drosophila melanogaster*, together with high-quality pixel-wise instance segmentations of individual neurons. To the best of our knowledge, FISBe constitutes the first publicly available real-world benchmark dataset for instance segmentation of wide-spanning, thin filamentous and tightly interweaving objects. Top row: Exemplary FISBe images (3d) visualized in 2d via maximum intensity projection (MIP). Bottom row: Corresponding 2d projections of ground truth instance segmentation masks (3d).

Abstract

Instance segmentation of neurons in volumetric light microscopy images of nervous systems enables groundbreaking research in neuroscience by facilitating joint functional and morphological analyses of neural circuits at cellular resolution. Yet said multi-neuron light microscopy data exhibits extremely challenging properties for the task of instance segmentation: Individual neurons have long-ranging, thin filamentous and widely branching morphologies, multiple neurons are tightly inter-weaved, and partial volume effects, uneven illumination and noise inherent to light microscopy severely impede local disentangling as well as long-range tracing of individual neurons. These properties reflect a current key challenge in ma-

chine learning research, namely to effectively capture long-range dependencies in the data. While respective methodological research is buzzing, to date methods are typically benchmarked on synthetic datasets. To address this gap, we release the FlyLight Instance Segmentation Benchmark (FISBe) dataset, the first publicly available multi-neuron light microscopy dataset with pixel-wise annotations. In addition, we define a set of instance segmentation metrics for benchmarking that we designed to be meaningful with regard to downstream analyses. Lastly, we provide three baselines to kick off a competition that we envision to both advance the field of machine learning regarding methodology for capturing long-range dependencies, and facilitate scientific discovery in basic neuroscience. Project page: <https://kainmueller-lab.github.io/fisbe>

1. Introduction

Most existing instance segmentation benchmarks in computer vision are collections of natural images [10, 41, 77]. These are often suitably addressed with proposal-based methods like Mask R-CNN [25, 28], as the assumption that shapes of objects are well approximated by bounding boxes mostly holds. However, this key assumption is violated in a range of highly relevant application domains, including neuroscience [21, 74], the domain the FISBe dataset we contribute in this work stems from. Here, objects can span large parts of an image and have complex (e.g., tree-like) and intertwined shapes. Consequently, multiple instances may have very similar, very large bounding boxes.

Benchmarks from the neuroscientific domain, namely on neuron instance segmentation in electron microscopy (EM) data [1], have greatly facilitated the development of instance segmentation methodology that is applicable in the face of complex, wide-ranging object shapes. Beyond sophisticated object shapes, said benchmarks also call for methodology that applies to very large images, way beyond what current GPU memory can hold [21, 72]. On these benchmarks, proposal-free methods based on CNN backbones [7, 11, 22, 37, 38, 75] constitute the current state of the art, and mostly also lend themselves to arbitrarily large images thanks to tile-and-stitch inference.

However, an object category that generally renders image segmentation very challenging is not represented in the above-mentioned benchmarks, namely objects that exhibit very thin (down to single-pixel width), filamentous structures. Benchmarks have been established for *semantic* segmentation of very thin filamentous structures in a range of real-world applications, including neuron segmentation in light microscopy (LM) data [3, 49, 57], blood vessel segmentation in various medical imaging modalities [44, 66], and road extraction from satellite imagery [2, 16]. However, respective *instance* segmentation benchmarks are currently lacking despite the high relevance of the task, e.g., in basic neuroscience [51]. The closest related publicly available dataset that exhibits thin and complex object shapes is [74]. Yet it lacks tightly inter-weaved objects by design, and furthermore does not come with pixel-wise ground truth segmentations nor recommended metrics for benchmarking.

Consequently, there is at present a lack of methodology applicable for instance segmentation of wide-ranging thin filamentous intertwined shapes: Only very few deep-learning approaches are potentially suitable, among which Flood Filling Networks [30] and PatchPerPix [47]. Most proposal-free instance segmentation methods do not appear suitable: Three-label models [4] degenerate in the face of very thin instances because their interior equals their boundary; models predicting pixel affinities [18, 70] become inappropriate if they rarely encounter foreground in their fixed pixel neighborhoods (as compared to the dense-

foreground EM data they were designed for); metric learning models [7, 11] lack the capacity to capture long-range connectivity beyond their receptive fields. Likewise, methods proposed specifically for cell instance segmentation do not appear suitable: Cellpose [67] assumes locally (i.e., within receptive field) visible cues towards some semantically meaningful center point which does not hold true for our dataset; Stardist [73] employs star-convex polygons/polyhedrons as proposals, which do not provide viable approximations of neurons. As for non-learned, application-specific methods for neuron separation, some approaches rely on user-defined [62] or pre-detected anchor points, in particular on cell body detection [40, 59, 78]. This renders these methods not directly applicable to our data, where cell bodies may lie outside of the imaged volume (namely in the ventral nerve cord). Other non-learned application-specific approaches are based on color clustering [14, 68], which is technically applicable, yet the underlying assumption that each neuron has a unique color is often violated on our data.

A promising recent alternative are query-based methods [6, 8, 35], which operate without explicit prior assumptions on object sizes or shapes. However, e.g., SAM [35] is not directly applicable as it has not yet been extended to full 3d and it is unclear if and how tile-and-stitch prediction, as would be necessary given the size of individual FISBe images, could be achieved in a seamless manner. We deem respective potential extensions of SAM a very interesting research topic for which, albeit out of scope, FISBe can serve as benchmark. Further recent trends towards explicit modelling of long-range data dependencies appear promising [26, 36, 55], yet so far these models have only been benchmarked on synthetic data [33, 42], sequence data [69], and image classification [12], and thus, their potential for improving instance segmentation of long, complex, intertwined objects in real-world tasks has not been assessed.

Our work addresses the gap that, to date, solely synthetic data is available to facilitate methods development towards capturing long-range data dependencies. To this end, we herewith release the FISBe dataset, a 3d multicolor light microscopy dataset of wide-ranging and tightly inter-weaving neuronal morphologies in the brain of the fruit fly *Drosophila melanogaster*, together with high quality expert instance segmentations of individual neurons. The dataset comprises 101 large, expert-labeled 3d images, of which 30 are completely- and 71 partly labeled, with a total of ~ 600 pixel-wise neuron instance masks. Exemplary images and instance masks are shown in Fig. 1. The novelty of our data entails a gap in evaluation metrics: Metrics commonly employed for benchmarking instance segmentation methodology do not appropriately account for the long, very thin and filamentous object shapes; e.g., mean average precision (mAP) with pixel-level IoU for localization is not appropriate for thin structures [46, 64]. Thus standard metrics may

not provide meaningful quantification of segmentation performance. To this end, we identify a set of informative evaluation metrics, and contribute a novel aggregate score that we recommend for method benchmarking. Given our metrics, we evaluate three baseline methods, namely the two learnt methods that are, to our knowledge, technically able to handle the intricacies of our data to date [30, 47], as well as one non-learnt application-specific method that is technically applicable [14]. In summary, we contribute:

- The FISBe dataset, to our knowledge the first public benchmark dataset for instance segmentation of real-world, wide-ranging, thin filamentous and tightly interweaving objects.
- A set of metrics and a novel ranking score for respective meaningful method benchmarking.
- An evaluation of three baseline methods in terms of the above metrics and score.

Concerning the size of our dataset, on the one hand, latest 2d natural image datasets are orders of magnitude bigger than ours [35] and thus pave the way for particularly data-hungry methods development. Such size is, however, far beyond reach for 3d data, let alone for data from the life sciences where expert knowledge is required for annotation, and acquiring pixel-wise ground truth for image data alike ours has been deemed difficult or infeasible in related work [14, 20]. On the other hand, numerous benchmark datasets similarly sized as FISBe have proven to greatly boost methods development in the machine learning community, and have likewise boosted respective application-specific scientific discovery [21, 32, 72]. We thus foresee our work to be of impact both in advancing the field of machine learning regarding methodology for capturing long-range data dependencies, and in streamlining cell-level analyses of brain function towards advances in basic neuroscience. We release our data through zenodo (<https://zenodo.org/doi/10.5281/zenodo.10875063>) and our project page <https://kainmueller-lab.github.io/fisbe>.

2. Dataset

The FISBe dataset consists of 101 3d multicolor LM images of the central nervous system of the fruit fly *Drosophila melanogaster*. The images originate from a large pre-existing resource of LM acquisitions [51]. Similar data has already contributed to breakthrough neuroscientific findings, e.g., towards a mechanistic understanding of memory formation and -retrieval in *Drosophila* on a cellular level [13]. Our work aims at facilitating such findings at scale. For a more elaborate introduction to the biological background of our data, we refer the interested reader to Suppl. Sec. A.4. In the following, we describe the imaging resource FISBe stems from in Sec. 2.1, the selection and annotation process for our dataset in Sec. 2.2, and recommended data splits and evaluation for benchmarking in Sec. 2.3.

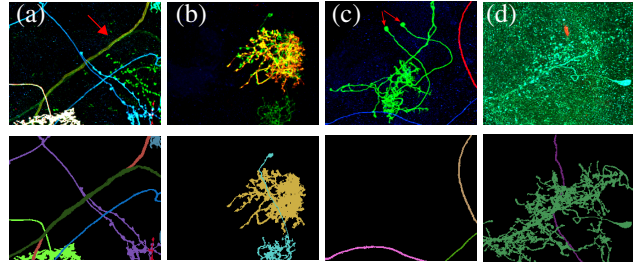


Figure 2. Exemplary challenging cases for disentangling neurons in FISBe images (top row), and respective expert annotations (bottom row). (a) Long overlap of two neurons running in parallel, (b) two almost completely overlapping neurons in different color (only one could successfully be annotated), (c) two inter-woven neurons of same color that could not be separated (clearly identified by two somata), and (d) dim neuron in noisy background.

2.1. Image Data Acquisition and Characteristics

Our dataset originates from the FlyLight project [51], where confocal microscopy images of the nervous systems of $\sim 74,000$ flies were acquired with a technique called MultiColor FlpOut (MCFO) [54]. This image collection was previously released¹. We selected images from the "40x Gen1" subset where images have an isotropic resolution of $0.44\mu m$, an average size of $\sim 400 \times 700 \times 700$ pixels, and three color channels. Fig. 1 (top row) shows exemplary MCFO images. Note that visualizations of image data shown in this paper are maximum intensity projections along the z axis, if not noted otherwise. For exemplary orthographic views see Suppl. Fig. 9. For more information on the dataset see our datasheet [23] in Suppl. Sec. A.1.

MCFO images capture the very thin, tree-like morphology of individual neurons as well as the intertwining of multiple neurons. The number of neurons expressed in individual images varies from extremely dense (>50) to very sparse (1-2). The FlyLight project has sorted images into five categories according to expression density, where 18% of images express up to 10 neurons (cat. 1 and 2) and 55% express around 20 neurons (cat. 3, cf. Suppl. Fig. 1 in [51]).

MCFO imagery has sparse, unbalanced foreground signal, low signal-to-noise ratio, and exhibits artifacts like broken structures and intensity shifts. Intensity varies strongly, per image, per neuron and within neurons. Thus neurons may appear in very different quality, ranging continuously from clearly visible neurons to very dim neurons that are partly indistinguishable from noise. The MCFO technique causes individual neurons to exhibit random colors, though color diversity per image is often not sufficient to allow for distinguishing all neurons by color. Multiple neurons in very close proximity may appear as overlapping due to partial volume effects². Neurons in MCFO images are par-

¹Download (CC BY 4.0 license): <https://gen1mcfo.janelia.org>

²Multiple instances occupy the same 3d pixel (distinct from occlusion)

ticularly hard to distinguish if neurons of same or similar color form dense clusters or overlap (see Fig. 2).

2.2. Image Selection and Labeling Process

Labeling 3d data is generally cumbersome as objects often need to be viewed with different angles, scales and color settings. As for the FlyLight data, limited resolution inherent in confocal microscopy makes isolating individual similarly colored, close-by neurons particularly difficult. Furthermore, in some cases poor signal-to-noise ratio makes it difficult to identify the complete wide-spanning extent of neurons. In both cases, expert anatomical knowledge of fruit fly neurons is often crucial for successful annotation.

To form FISBe, expert annotators chose 101 samples from the FlyLight data for which they determined by eye that manual annotation is feasible. Compared to the full FlyLight resource, this introduces a bias in our dataset towards sparser expression densities: Of our 101 images, one image is of density cat. 1, 72 are of cat. 2, and 28 of cat. 3. Two expert annotators manually segmented and proof-read each other to label as many neurons as possible in these 101 images using the interactive rendering tool VVD Viewer[65]. Annotators were able to segment a total of 590 neurons. Labeling a single neuron took 30-60 min on average, yet for a difficult neuron it could take up to 4 hours. Not every neuron in every sample could be annotated successfully, thus yielding completely- as well as partly labeled images. A third annotator performed a final visual inspection of all labeled neurons and revised the categorization into completely- and partly labeled images.

Our completely labeled dataset comprises 30 MCFO images and a total of 139 labeled neurons; see Fig. 1 (1st and 2nd example) and Suppl. Fig. 10. Our partly labeled dataset comprises 71 MCFO images and a total of 451 labeled neurons; see Fig. 1 (3rd and 4th example) and Suppl. Fig. 12. These images exhibit unlabeled neuronal morphologies because expert annotators were either unable to disentangle multiple neurons of the same color in a dense cluster, or unable to annotate very dim neurons that are partly indistinguishable from noisy background. Note, 61 images contain labeled neurons that overlap due to partial volume effects.

Complementing our new annotated data, the large trove of previously released non-annotated images in the FlyLight resource may serve for self-supervised pre-training.

2.3. Benchmarking Setup

We split the completely labeled data into train, validation and test sets with 18, 5 and 7 samples respectively as defined in Suppl. Table 5. We split the partly labeled data into train, validation and test sets with 43, 12 and 16 samples respectively as defined in Suppl. Table 6. We recommend evaluation on the combined data (i.e., the union of completely and partly labeled data) as the main benchmark-

ing scenario. To assess training stability, we recommend to report summary statistics over three training runs in each evaluated scenario.

3. Evaluation Metrics

Our dataset constitutes the first benchmark dataset for *instance* segmentation of thin filamentous structures. Consequently, we need to assess which evaluation metrics are suitable for benchmarking. The main requirements for a suitable metric are: (r1) To account for thin filamentous structures, (r2) to be able to handle overlapping instances (both in ground truth and predicted instances), and (r3) to be meaningful with respect to downstream tasks.

Some existing benchmarks for *semantic* segmentation of filamentous structures have employed topology-based metrics, which assess the similarity between graph representations of ground truth- and predicted objects [2, 24]. We deem these not suitable for our data, as obtaining topologically correct (tree) graph representations of neurons is infeasible due to the limited resolution of light microscopy.

Instead, we follow the Metrics Reloaded [46] recommendation for thin filamentous instance segmentation and apply an instance-level F1 score as one of our main evaluation metrics. Moreover, we propose to complement the F1 score with a custom metric that we design towards satisfying r3, namely a centerline recall with one-to-many matching, which we refer to as *average ground truth coverage*. We combine both metrics to derive an aggregate benchmark score. Finally, we define a set of easily interpretable error measures that may provide additional insight to methods developers and practitioners. E.g., we extend existing work [5, 50] by defining false split (FS) and false merge (FM) error counts for overlapping instances. We define our selected metrics in Sec. 3.1, ensuring that all apply not only to completely- but also to partly labeled data, and discuss properties and suitability in Sec. 3.2. Suppl. Table 2 summarizes all metrics with their localization and matching.

3.1. Metrics Definitions

Instance segmentation can be phrased as a pixel labeling problem, where pixels with same label form instances. Note that in FISBe, one pixel can be assigned multiple labels due to overlapping instances. Segmentation quality is generally assessed via evaluation metrics that capture how well predicted instances overlay with given ground truth (gt) instances. We denote a set of gt instances $G = \{g_k\}_{k \in L_G}$ and a set of predicted instances $P = \{p_l\}_{l \in L_P}$ where L_G and L_P represent the sets of labels identifying gt and predicted instances, and $|G|$ and $|P|$ denote the total number of instances of the respective set. With subscript i the set is limited to a single image, e.g., G_i , otherwise it refers to the set over all images I . Gt- and prediction sets exclude background (bg) as instance label if not stated otherwise.

Average F1 score $avF1$. Following [46], a metric consists of three steps: localization, matching and computation. The localization step employs some function to compute how well each pair of predicted and gt instances are co-localized. The matching step selects subset of these pairs, resulting in a match of predicted to gt instances. The computation step computes the value of the metric based on the quality of the previously computed subset of matched instances.

It has been shown that pixel-level IoU or F1 are not suitable for thin structures as small variations on boundaries can have a large effect [17, 46]. Thus we employ $clDice$ [64], a variation of the Dice score that operates on object centerlines, for the localization step. Following [64], we use medial surface axial thinning algorithm [39] to skeletonize volumetric instance masks and denote it with function $skeletonize(\cdot)$. Given ground truth and prediction we compute $clDice$ as follows:

$$clPrecision(p, g) = \frac{|skeletonize(p) \cap g|}{|skeletonize(p)|} \quad (1)$$

$$\forall p \in P_i, \forall g \in G_i \cup \{bg\}$$

$$clRecall(g, p) = \frac{|skeletonize(g) \cap p|}{|skeletonize(g)|} \quad (2)$$

$$\forall g \in G_i, \forall p \in P_i \cup \{bg\}$$

$$clDice(g, p) = 2 * \frac{clPrecision(p, g) * clRecall(g, p)}{clPrecision(p, g) + clRecall(g, p)} \quad (3)$$

$$\forall g \in G_i, \forall p \in P_i$$

$clDice$ is only computed for foreground pairs as we do not skeletonize the background, but we, e.g., include it for $clPrecision$ to detect predictions mainly located in the gt background.

For the matching step we follow the greedy strategy recommended in [46]. To this end we compute $clDice$ for all pairs of predicted and gt instances $\{clDice(p, g) \mid \forall i \in I : \forall p \in P_i, \forall g \in G_i\}$. We iterate through all scores in descending order and match the corresponding (p, g) -pair if neither has been assigned before. Similarly to [50], we denote $p \in g$, if the two instances have been matched. In the computation step, we derive true positives (TP), false positives (FP) and false negatives (FN) for all $clDice$ thresholds th in the range $[0.1, 0.9]$ with step size 0.1:

- TP: all predicted instances that are assigned to a gt instance with $clDice > th$:

$$TP = |\{p \in P \mid \exists g : p \in g \wedge clDice(p, g) > th\}|$$

- FP: all unassigned predicted instances $FP = |P| - TP$
- FN: all unassigned gt instances $FN = |G| - TP$

Based on these values we compute the F1 score $F1 = \frac{2TP}{2TP+FP+FN}$ for each threshold. Note that TP, FP, FN are thus computed across all images. The final $avF1$ score is the average of all F1 scores.

Average ground truth coverage C . We compute $clPrecision$ scores for all pairs of predicted and gt instances as localization criterion. We match each prediction to the gt instance with the highest $clPrecision$ score (one-to-many matching). Then we average $clRecall$ for all gt instances and the union of their matched predictions (to avoid double-counting of pixels with overlapping predictions):

$$C = 1/|G| \sum_{g \in G} clRecall(g, \bigcup_{\forall p \in P: p \in g} p) \quad (4)$$

Aggregate benchmark score S . We propose to combine the average F1 score $avF1$ and the average ground truth coverage C to form a primary benchmark ranking score S . We average both measures to obtain the final ranking score: $S = 0.5avF1 + 0.5C$. Note that we do not multiply them, as a linear increase in segmentation quality should lead to linear increase in the score function [17].

False splits FS and false merges FM . False split errors occur if one gt instance is covered by multiple predicted instances. False merge errors occur if one predicted instance covers more than one gt instance. We propose to use a greedy many-to-many matching algorithm that naturally handles overlapping instances and based on which we can compute FM and FS directly in a unified way. For the matching, we iteratively assign predicted and gt instances with the highest $clRecall$ value while keeping track of already matched pixels (see Algorithm 1). Remaining $clRecall$ values are constantly updated to only include *free* pixels, which are available for further matching. By doing so, we avoid that predicted instances in overlapping gt regions are assigned multiple times; or that mostly overlapping predicted instances are assigned to the same gt instance (see Suppl. Fig. 5). Note that we monitor centerline pixels for gt instances and complete pixelwise masks for predicted instances due to the definition of $clRecall$.

We then count for each gt instance the additional number of assigned predicted instances apart from one correctly matched instance to compute false splits (with $th = 0.05$)

$$FS = \sum_{g \in G} \max((\sum_{p \in P: p \in g} 1) - 1, 0), \quad (5)$$

and analogously for false merges (with $th = 0.1$)

$$FM = \sum_{p \in P} \max((\sum_{g \in G: g \in p} 1) - 1, 0). \quad (6)$$

True positives $clDice$. We report average centerline Dice for uniquely matched instances $clDice_{TP}$ to provide a measure of how well true positives are reconstructed. We re-use the matching computed for $avF1$, employ a threshold of 0.5 for the definition of TP and define

$$clDice_{TP} = \frac{1}{|TP_{0.5}|} \sum_{(p, g): p \in TP_{0.5} \wedge p \in g} clDice(p, g). \quad (7)$$

Algorithm 1: Greedy Many-to-many Matching

input : G : set of gt instances g_k ,
 P : set of predicted instances p_l ,
th: cIRecall threshold
output: M : set of matched (g_k, p_l) -instances

initialize $M \leftarrow \emptyset$
initialize $G_{\text{free}} \leftarrow \{\text{skeletonize}(g_k) \mid \forall g_k \in G\}$
initialize $P_{\text{free}} \leftarrow \text{copy}(P)$
 $\text{cIR} \leftarrow \text{sort}(\{\text{cIRecall}(\text{skeletonize}(g_k), p_l) \mid \forall g_k \in G, \forall p_l \in P\}, \downarrow)$

while $\text{top}(\text{cIR}) > \text{th}$ **do**

$g_k, p_l \leftarrow \text{pop}(\text{cIR})$
 $M += \{(g_k, p_l)\}$
update $g_{\text{free}_k} \leftarrow g_{\text{free}_k} \setminus p_l$
update $p_{\text{free}_l} \leftarrow p_{\text{free}_l} \setminus g_k$
forall $(g_m, p_n) \in \text{cIR}$ **do**

if $g_m = g_k$ **then**

$\text{update } \text{cIR}(g_m, p_n) = \frac{|g_{\text{free}_m} \cap p_n|}{|\text{skeletonize}(g_m)|}$

if $p_n = p_l$ **then**

$\text{update } \text{cIR}(g_m, p_n) = \frac{|\text{skeletonize}(g_m) \cap p_{\text{free}_n}|}{|\text{skeletonize}(g_m)|}$

$\text{sort}(\text{cIR}, \downarrow)$

Evaluating partly labeled samples. In partly labeled samples only a subset of neurons is annotated. For unlabeled pixels we do not know if there is background or other neuronal structures and for labeled neurons if they partly overlap with a non-annotated one. This has no influence on average ground truth coverage as well as false split and false merge counts, although the reported measures only reflect parts of the whole volume. However, for the F1 score the false positive count cannot be computed. Therefore, we only count predicted instances that are not one-to-one matched based on cIDice, but that primarily lie within a gt instance and not the background:

$$\text{FP}_{\text{partly}} = |\{p \in P \mid \nexists g : p \in g \wedge \arg \max_{g \in G \cup \{\text{bg}\}} \text{cIPrecision}(p, g) \neq \text{bg}\}| \quad (8)$$

We use this error count as an approximation of false positives and adapt the formula to $F1 = \frac{2\text{TP}}{2\text{TP} + \text{FP}_{\text{partly}} + \text{FN}}$. All other calculation steps remain unchanged. Note that thus the F1 scores of completely and partly labeled image sets cannot be compared directly. To evaluate the full dataset, we average the results for the completely and partly labeled set (for normalized measures, counting measures such as FS, FM and TP are summed up).

Evaluating challenging cases. Main challenges are dim and overlapping neurons (cf. Fig. 2). To evaluate how well such subsets of neurons are segmented, we report gt cover-

age C and the relative number of TPs ($\text{tp} = \frac{\text{TP}_{S,0.5}}{|G_S|}$, with greedy one-to-one matching and $\text{cIDice} > 0.5$) for the respective subsets ($G_{\text{dim}}/G_{\text{ovlp}}$). Dim neuron instances of validation and test sets are listed within the dataset.

3.2. Discussion

We satisfy requirement (r1) by using cIPrecision, cIRecall and cIDice in all of our measures. They are defined in such a way that they handle overlaps in both predicted and gt instances, thus satisfying requirement (r2).

The *avF1* score considers all error types equally. However, FP and FS errors are more likely to occur in MCFO segmentations due to low signal-to-noise ratio and broken structures. They are often induced by only a limited number of incorrect pixels, whereas FN errors are limited by the number of neurons and require that all or large parts of neurons are missing. This can lead to disproportionately low scores that do not reflect how we would visually rate segmentation quality (see Fig. 3 (a)+(b)).

To mitigate this, we complement the *avF1* score by the average gt coverage C , resulting in an improved balancing of the different types of errors. C provides an intuitive way for measuring how comprehensively gt instances are segmented by the model. C strongly penalizes FN and FM errors, an important property for downstream tasks. Consider the edge case of a perfect foreground segmentation. If FM are not penalized, assigning the same label to each connected component would lead to a perfect score, despite merges occurring at every overlap and point of contact. Thus, as desired, if a model achieves to split a previously occurring FM correctly, this will lead to a large improvement as an additional gt instance will get matched (see Fig. 3 (c)).

However, C does not incorporate FP and FS errors. Consider the same edge case as before, but now we assign a separate instance label to each foreground pixel. This, as a consequence of the one-to-many matching still leads to a perfect score for C . But the *avF1* score will be exceedingly low. Similarly if the gt instances are indeed segmented perfectly, but the outside noise is segmented as well (see Fig 3 (d)). Note that this highlights why C should not be used as a standalone metric. FP and FS errors are accounted for by the *avF1* score, and C penalizes FN and FM errors. Thus C and *avF1* nicely complement each other. For additional edge cases and the corresponding quantitative evaluation please see Suppl. Fig. 6.

Concerning (r3) there are two highly relevant downstream tasks we took into account: 1. Morphological analysis of neurons, and 2. the task of searching for a given neuronal morphology within all MCFO images. For the first task neurons of interest need to be reconstructed in their entirety. In this regard, FN and only partly annotated neurons are critical, as their manual curation is very time-consuming. FP, FM and FS are less relevant as, up

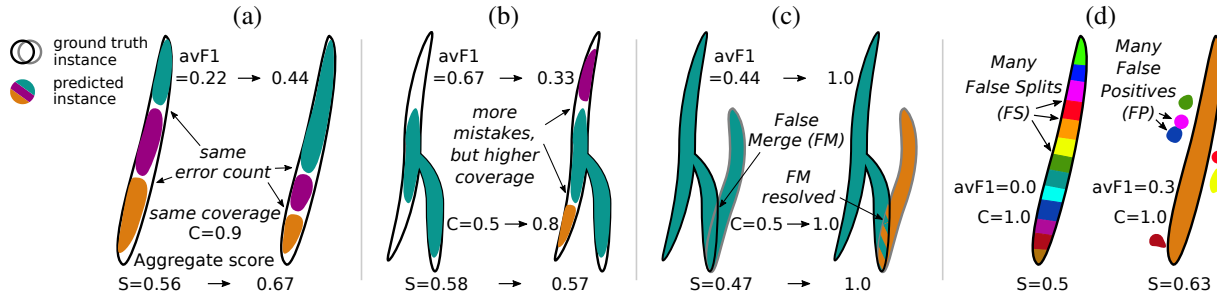


Figure 3. Visualization of segmentation examples to assess suitable evaluation metrics: (a) Depending on the split position, avF1 can vary significantly at identical gt coverage and error count. (b) Using the avF1 score alone would favor lower coverage over more false split errors. This might be disadvantageous in downstream analysis tasks. In (c) resolving the merge leads to a large improvement in the overall score. In (d) both cases achieve a perfect score wrt. the gt coverage C . By penalizing FP and FS errors in the F1 score the limitations of these predictions are reflected in the overall score. For more edge cases and the full quantitative numbers please see Suppl. Fig. 6.

to a point, they can relatively easily be corrected with a few clicks. This importance of completeness is strongly reflected in C . For the second task, the above considerations still hold, except that FP are more problematic. This is accounted for by the F1 score, which, as the number of FP can often be much higher than the number of TP and FN (see Table 1), heavily penalizes such cases.

Overall, our benchmark score S is in accordance with all our requirements. However, as a single benchmark score most likely cannot do justice to every possible use case, we report additional metrics that can be resorted to for alternative downstream tasks as well as for considerations on method improvements. The additional metrics all satisfy r1 and r2. Finally, our proposed many-to-many matching algorithm is very generic, despite adhering to our quite specific requirements. There is no special treatment of overlapping regions which strongly facilitates the matching. The algorithm can be applied to other object shapes by replacing cIRecall with other overlap-based metrics like IoU or IoR.

4. Baselines

To showcase the FISBe dataset together with our selection of metrics, we provide evaluation results for three baseline methods, namely PatchPerPix [47], Flood Filling Network (FFN) [29, 30] and a non-learned application-specific color clustering from Duan et al. [14, 68]. For information on all models, including training and validation details, see Suppl. Sec. A.3. Quantitative results for the full dataset are shown in Table 1, for completely and partly sets in Suppl. Table 3 and 4. Qualitative results are shown in Fig. 4, Suppl. Fig. 7 and 8. The results show that all three baseline methods yield large fragments for clearly visible and easily separable neurons. There are, however, many segmentation errors as reflected by the low avF1 scores (maximum value of $0.34_{\pm 0.01}$). PatchPerPix achieves best results for all metrics, except for false merges. Inspecting PatchPerPix results visually shows that many touching neurons are falsely merged even with different color. FFNs and Duan et al. perform similar, al-

though Duan et al. has the highest number of false splits and lowest number of false merges. Thus it separates best touching neurons.

As the training of PatchPerPix is not directly applicable to the partly labeled data we only report results for models trained on the completely labeled data. FFNs, on the other hand, operate in a one-versus-all fashion and can thus by design train on partly labeled data without any modifications. Training FFN on the full dataset shows increases in all metrics, especially on the test set. PatchPerPix intrinsically handles overlapping instances but it can only bridge small overlaps up to the used patch size. FFN does not support overlaps out of the box but could, with some modifications for efficient inference, be extended to this end. None of the learnt methods models long-range data dependencies. In summary, all three baseline methods do yield some true positive neuron reconstructions, but extensive further method development is necessary to be able to achieve high quality instance segmentation on this dataset.

5. Conclusion

With this work we release the FISBe dataset, which is, to the best of our knowledge, the first real-world benchmark dataset for instance segmentation of wide-ranging thin filamentous intertwined objects. In addition to the data we contribute a set of metrics for meaningful method benchmarking and three baselines. A limitation of FISBe is its bias towards sparser samples from the FlyLight MCFO image resource it stems from. This entails that in general, benchmarking on FISBe does not serve to gauge method performance on denser samples. A possible avenue to mitigate this issue is to define proxy evaluation metrics on denser samples with the help of domain-specific downstream tasks for which higher-level annotations exist (see Sec. 3.2 for examples of such tasks). Main limitations of our baseline methods are that they handle no or only small overlaps and are computationally very demanding. In future work, we are excited to see recently proposed methods for

Table 1. Quantitative results on the full FISBe validation and test sets (i.e., completely and partly labeled data combined; for results on the respective subsets see Suppl. Table 3). We compare PatchPerPix (ppp, [47]), Flood Filling Networks (FFN, [30]) trained on the completely labeled and the full training dataset (+partly) and Duan et al.’s color clustering [14]. We report mean and standard deviation (\pm) over three independent runs (except for Duan et al.’s as it is non-learned). For all scores except FS and FM higher values are better.

Split Method	S	$avF1$	C	$clDice_{TP}$	FS	FM	C_{dim}	C_{ovlp}	tp	tp_{dim}	tp_{ovlp}	
Val	ppp	0.38 \pm 0.02	0.41 \pm 0.02	0.35 \pm 0.01	0.75 \pm 0.02	6.0 \pm 0.8	24 \pm 1.6	0.12 \pm 0.01	0.38 \pm 0.04	0.46 \pm 0.01	0.16 \pm 0.04	0.39 \pm 0.03
	FFN	0.25 \pm 0.01	0.27 \pm 0.01	0.23 \pm 0.01	0.79 \pm 0.01	7.0 \pm 2.9	12 \pm 2.0	0.03 \pm 0.01	0.30 \pm 0.01	0.32 \pm 0.01	0.04 \pm 0.01	0.37 \pm 0.02
	FFN+partly	0.27 \pm 0.01	0.29 \pm 0.01	0.24 \pm 0.01	0.79 \pm 0.01	7.7 \pm 2.6	14 \pm 0.8	0.02 \pm 0.01	0.33 \pm 0.02	0.34 \pm 0.03	0.03 \pm 0.00	0.38 \pm 0.04
	Duan et al.	0.24	0.26	0.22	0.70	14	13	0.02	0.28	0.37	0.03	0.42
Test	ppp	0.35 \pm 0.00	0.34 \pm 0.01	0.35 \pm 0.01	0.80 \pm 0.00	19 \pm 2.9	52 \pm 3.4	0.16 \pm 0.03	0.27 \pm 0.04	0.36 \pm 0.01	0.19 \pm 0.04	0.19 \pm 0.03
	FFN	0.25 \pm 0.03	0.22 \pm 0.04	0.29 \pm 0.02	0.80 \pm 0.01	17 \pm 1.7	39 \pm 5.3	0.03 \pm 0.01	0.26 \pm 0.03	0.32 \pm 0.03	0.00 \pm 0.00	0.24 \pm 0.05
	FFN+partly	0.27 \pm 0.01	0.24 \pm 0.02	0.31 \pm 0.00	0.80 \pm 0.01	18 \pm 3.7	36 \pm 3.6	0.04 \pm 0.01	0.28 \pm 0.01	0.36 \pm 0.01	0.03 \pm 0.00	0.28 \pm 0.01
	Duan et al.	0.30	0.27	0.33	0.77	45	29	0.03	0.36	0.37	0.03	0.34

Test	$F1_{0.1}$	$F1_{0.2}$	$F1_{0.3}$	$F1_{0.4}$	$F1_{0.5}$	$F1_{0.6}$	$F1_{0.7}$	$F1_{0.8}$	$F1_{0.9}$
ppp	0.50 \pm 0.01	0.48 \pm 0.01	0.44 \pm 0.01	0.41 \pm 0.02	0.35 \pm 0.02	0.29 \pm 0.02	0.26 \pm 0.01	0.19 \pm 0.02	0.12 \pm 0.01
FFN	0.34 \pm 0.05	0.31 \pm 0.04	0.28 \pm 0.04	0.25 \pm 0.05	0.22 \pm 0.04	0.20 \pm 0.04	0.17 \pm 0.03	0.12 \pm 0.01	0.07 \pm 0.01
FFN+partly	0.36 \pm 0.02	0.32 \pm 0.02	0.30 \pm 0.02	0.27 \pm 0.03	0.25 \pm 0.03	0.21 \pm 0.03	0.18 \pm 0.02	0.15 \pm 0.02	0.09 \pm 0.01
Duan et al.	0.43	0.38	0.35	0.33	0.31	0.29	0.20	0.12	0.06

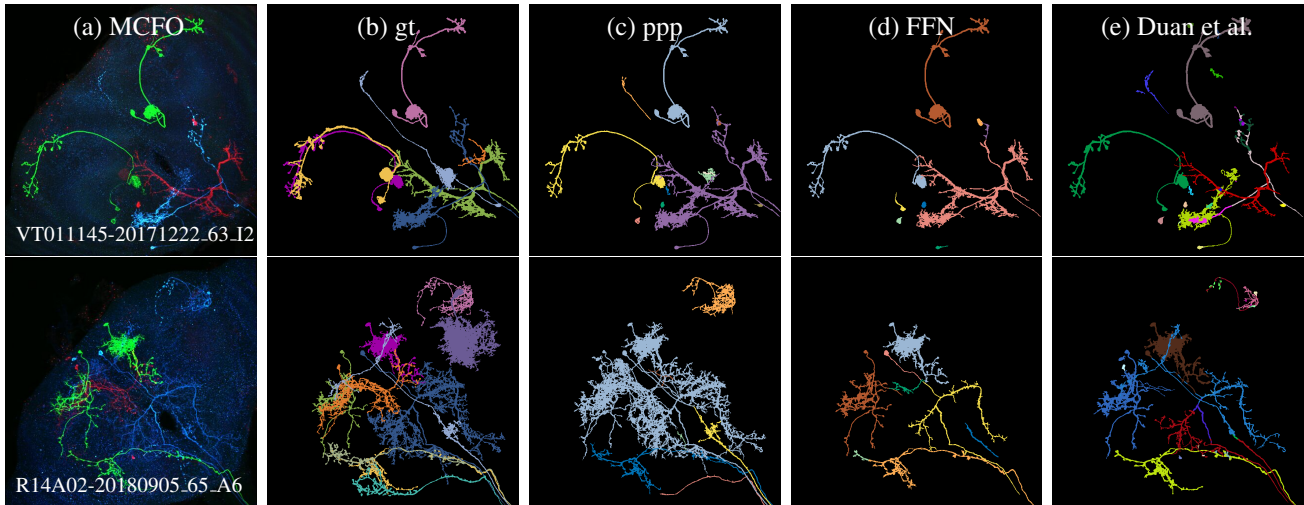


Figure 4. Qualitative results for our three baseline methods: PatchPerPix (ppp), Flood Filling Networks (FFN) and Duan et al.’s color clustering. In the top row all three methods yield few correctly segmented neurons (the two green neurons), but ppp and FFN merge the blue and the red one, and Duan et al.’s splits the blue neuron while nicely segmenting the red one. In the bottom row ppp merges many neurons of different color; FFN segments three neurons, but has low coverage; and Duan et al.’s also merges different colored neurons.

long-range data dependencies, such as structured state space models [26, 55] and continuous CNNs [36], applied to this real-world dataset. In addition, the huge set of already available non-annotated images should lend itself perfectly for self-supervised pretraining. We believe that the new challenging FISBe dataset is a great resource to the computer vision community as it might reveal blind spots of current methods. Thus, we hope that it will lead to new methods

development for capturing long range data dependencies, while at the same time advancing cell-level analyses in basic neuroscience.

Acknowledgements. We thank Aljoscha Nern for providing unpublished MCFO images as well as Geoffrey W. Meissner and the entire FlyLight Project Team for valuable discussions. P.H., L.M. and D.K. were supported by the HHMI Janelia Visiting Scientist Program.

References

- [1] Ignacio Arganda-Carreras, Srinivas C Turaga, Daniel R Berger, Dan Cireşan, Alessandro Giusti, Luca M Gambardella, Jürgen Schmidhuber, Dmitry Laptev, Sarvesh Dwivedi, Joachim M Buhmann, et al. Crowdsourcing the creation of image segmentation algorithms for connectomics. *Frontiers in neuroanatomy*, 9:142, 2015. [2](#)
- [2] F. Bastani, S. He, S. Abbar, M. Alizadeh, H. Balakrishnan, S. Chawla, S. Madden, and D. DeWitt. Roadtracer: Automatic extraction of road networks from aerial images. In *2018 IEEE/CVF Conference on Computer Vision and Pattern Recognition (CVPR)*, pages 4720–4728, Los Alamitos, CA, USA, 2018. IEEE Computer Society. [2](#), [4](#)
- [3] Kerry M Brown, Germán Barrionuevo, Alison J Canty, Vincenzo De Paola, Judith A Hirsch, Gregory S X E Jefferis, Ju Lu, Marjolein Snippe, Izumi Sugihara, and Giorgio A Ascoli. The DIADEM data sets: representative light microscopy images of neuronal morphology to advance automation of digital reconstructions. *Neuroinformatics*, 9(2-3):143–157, 2011. [2](#)
- [4] Juan C. Caicedo, Jonathan Roth, Allen Goodman, Tim Becker, Kyle W. Karhohs, Matthieu Broisin, Csaba Molnar, Claire McQuin, Shantanu Singh, Fabian J. Theis, and Anne E. Carpenter. Evaluation of deep learning strategies for nucleus segmentation in fluorescence images. *Cytometry Part A*, 95(9):952–965, 2019. [2](#)
- [5] Juan C. Caicedo, Jonathan Roth, Allen Goodman, Tim Becker, Kyle W. Karhohs, Matthieu Broisin, Csaba Molnar, Claire McQuin, Shantanu Singh, Fabian J. Theis, and Anne E. Carpenter. Evaluation of deep learning strategies for nucleus segmentation in fluorescence images. *Cytometry Part A*, 95(9):952–965, 2019. [4](#)
- [6] Nicolas Carion, Francisco Massa, Gabriel Synnaeve, Nicolas Usunier, Alexander Kirillov, and Sergey Zagoruyko. End-to-end object detection with transformers. In *Computer Vision – ECCV 2020*, pages 213–229, Cham, 2020. Springer International Publishing. [2](#)
- [7] Long Chen, Martin Strauch, and Dorit Merhof. Instance segmentation of biomedical images with an object-aware embedding learned with local constraints. In *International Conference on Medical Image Computing and Computer-Assisted Intervention*, pages 451–459. Springer, 2019. [2](#)
- [8] Bowen Cheng, Alex Schwing, and Alexander Kirillov. Pixel classification is not all you need for semantic segmentation. *Advances in Neural Information Processing Systems*, 34:17864–17875, 2021. [2](#)
- [9] Özgün Çiçek, Ahmed Abdulkadir, Soeren S. Lienkamp, Thomas Brox, and Olaf Ronneberger. 3d u-net: Learning dense volumetric segmentation from sparse annotation. In *Medical Image Computing and Computer-Assisted Intervention – MICCAI 2016*, pages 424–432, Cham, 2016. Springer International Publishing. [19](#)
- [10] Marius Cordts, Mohamed Omran, Sebastian Ramos, Timo Rehfeld, Markus Enzweiler, Rodrigo Benenson, Uwe Franke, Stefan Roth, and Bernt Schiele. The cityscapes dataset for semantic urban scene understanding. In *Proc. of the IEEE Conference on Computer Vision and Pattern Recognition (CVPR)*, 2016. [2](#)
- [11] Bert De Brabandere, Davy Neven, and Luc Van Gool. Semantic instance segmentation with a discriminative loss function. *arXiv preprint arXiv:1708.02551*, 2017. [2](#)
- [12] Jia Deng, Wei Dong, Richard Socher, Li-Jia Li, Kai Li, and Li Fei-Fei. Imagenet: A large-scale hierarchical image database. In *2009 IEEE conference on computer vision and pattern recognition*, pages 248–255. Ieee, 2009. [2](#)
- [13] Michael-John Dolan, Ghislain Belliard-Guérin, Alexander Shakeel Bates, Shahar Frechter, Aurélie Lampin-Saint-Amaux, Yoshinori Aso, Ruairi JV Roberts, Philipp Schlegel, Allan Wong, Adnan Hammad, et al. Communication from learned to innate olfactory processing centers is required for memory retrieval in drosophila. *Neuron*, 100(3):651–668, 2018. [3](#)
- [14] Bin Duan, Logan A Walker, Douglas H Roossien, Fred Y Shen, Dawen Cai, and Yan Yan. Unsupervised neural tracing in densely labeled multispectral brainbow images. In *2021 IEEE 18th International Symposium on Biomedical Imaging (ISBI)*, pages 1122–1126, 2021. [2](#), [3](#), [7](#), [8](#), [19](#)
- [15] Erica Ehrhardt, Samuel C Whitehead, Shigehiro Namiki, Ryo Minegishi, Igor Siwanowicz, Kai Feng, Hideo Otsuna, FlyLight Project Team, Geoffrey W Meissner, David Stern, Jim Truman, David Shepherd, Michael H. Dickinson, Kei Ito, Barry J Dickson, Itai Cohen, Gwyneth M Card, and Wyatt Korff. Single-cell type analysis of wing premotor circuits in the ventral nerve cord of drosophila melanogaster. *bioRxiv*, 2023. [21](#)
- [16] Adam Van Etten, Dave Lindenbaum, and Todd M. Bacastow. Spacenet: A remote sensing dataset and challenge series. *CoRR*, abs/1807.01232, 2018. [2](#)
- [17] Adrien Foucart, Olivier Debeir, and Christine Decaestecker. Panoptic quality should be avoided as a metric for assessing cell nuclei segmentation and classification in digital pathology. *Scientific Reports*, 13(1):8614, 2023. [5](#)
- [18] C. Fowlkes, D. Martin, and J. Malik. Learning affinity functions for image segmentation: combining patch-based and gradient-based approaches. In *2003 IEEE Computer Society Conference on Computer Vision and Pattern Recognition, 2003. Proceedings.*, pages II–54, 2003. [2](#)
- [19] Shahar Frechter, Alexander Shakeel Bates, Sina Tootoonian, Michael-John Dolan, James Manton, Arian Rokkum Jamasb, Johannes Kohl, Davi Bock, and Gregory Jefferis. Functional and anatomical specificity in a higher olfactory centre. *eLife*, 8:e44590, 2019. [21](#)
- [20] Drew Friedmann, Albert Pun, Eliza L Adams, Jan H Lui, Justus M Kobschull, Sophie M Grutzner, Caitlin Castagnola, Marc Tessier-Lavigne, and Liqun Luo. Mapping mesoscale axonal projections in the mouse brain using a 3d convolutional network. *Proceedings of the National Academy of Sciences*, 117(20):11068–11075, 2020. [3](#)
- [21] J. Funke, E. Perlman, S. Turaga, D. Bock, and S. Saalfeld. Creml challenge, 2016. [2](#), [3](#)
- [22] Jan Funke, Fabian Tschopp, William Grisaitis, Arlo Sheridan, Chandan Singh, Stephan Saalfeld, and Srinivas Turaga. Large scale image segmentation with structured loss based

- deep learning for connectome reconstruction. *IEEE Transactions on Pattern Analysis and Machine Intelligence*, PP: 1–1, 2018. [2](#)
- [23] Timnit Gebru, Jamie Morgenstern, Briana Vecchione, Jennifer Wortman Vaughan, Hanna M. Wallach, Hal Daumé III, and Kate Crawford. Datasheets for datasets. *CoRR*, abs/1803.09010, 2018. [3](#), [13](#)
- [24] Todd A Gillette, Kerry M Brown, and Giorgio A Ascoli. The DIADEM metric: comparing multiple reconstructions of the same neuron. *Neuroinformatics*, 9(2-3):233–245, 2011. [4](#)
- [25] Ross Girshick, Jeff Donahue, Trevor Darrell, and Jitendra Malik. Rich feature hierarchies for accurate object detection and semantic segmentation. In *Proceedings of the 2014 IEEE Conference on Computer Vision and Pattern Recognition*, pages 580–587, Washington, DC, USA, 2014. IEEE Computer Society. [2](#)
- [26] Albert Gu, Karan Goel, and Christopher Ré. Efficiently modeling long sequences with structured state spaces. *CoRR*, abs/2111.00396, 2021. [2](#), [8](#)
- [27] gunpowder contributors. gunpowder: a library to facilitate machine learning on large, multi-dimensional images, 2019. [19](#)
- [28] Kaiming He, Georgia Gkioxari, Piotr Dollár, and Ross Girshick. Mask r-cnn, 2017. cite arxiv:1703.06870Comment: open source; appendix on more results. [2](#)
- [29] Michal Januszewski, Jeremy Maitin-Shepard, Peter Li, Jörgen Kornfeld, Winfried Denk, and Viren Jain. Flood-filling networks. *CoRR*, abs/1611.00421, 2016. [7](#), [19](#)
- [30] Michał Januszewski, Jörgen Kornfeld, Peter H. Li, Art Pope, Tim Blakely, Larry Lindsey, Jeremy Maitin-Shepard, Mike Tyka, Winfried Denk, and Viren Jain. High-precision automated reconstruction of neurons with flood-filling networks. *Nature Methods*, 15(8):605–610, 2018. [2](#), [3](#), [7](#), [8](#), [19](#)
- [31] Arnim Jenett, Gerald M. Rubin, Teri-T B. Ngo, David Shepherd, Christine Murphy, Heather Dionne, Barret D. Pfeiffer, Amanda Cavallaro, Donald Hall, Jennifer Jeter, Nirmala Iyer, Dona Fetter, Joanna H. Hausenfluck, Hanchuan Peng, Eric T. Trautman, Robert R. Svirskas, Eugene W. Myers, Zbigniew R. Iwinski, Yoshinori Aso, Gina M. DePasquale, Adrienne Enos, Phuson Hulamm, Shing Chun Benny Lam, Hsing-Hsi Li, Todd R. Laverty, Fuhui Long, Lei Qu, Sean D. Murphy, Konrad Rokicki, Todd Safford, Kshiti Shaw, Julie H. Simpson, Allison Sowell, Susana Tae, Yang Yu, and Christopher T. Zugates. A gal4-driver line resource for drosophila neurobiology. *Cell reports*, 2(4):991–1001, 2012. S2211-1247(12)00292-6[PII]. [14](#)
- [32] Yuanfeng Ji, Haotian Bai, Chongjian Ge, Jie Yang, Ye Zhu, Ruimao Zhang, Zhen Li, Lingyan Zhanng, Wanling Ma, Xiang Wan, et al. Amos: A large-scale abdominal multi-organ benchmark for versatile medical image segmentation. *Advances in Neural Information Processing Systems*, 35: 36722–36732, 2022. [3](#)
- [33] Junkyung Kim, Drew Linsley, Kalpit Thakkar, and Thomas Serre. Disentangling neural mechanisms for perceptual grouping. *CoRR*, abs/1906.01558, 2019. [2](#)
- [34] Diederik P. Kingma and Jimmy Ba. Adam: A method for stochastic optimization. *CoRR*, abs/1412.6980, 2014. [19](#)
- [35] Alexander Kirillov, Eric Mintun, Nikhila Ravi, Hanzi Mao, Chloe Rolland, Laura Gustafson, Tete Xiao, Spencer Whitehead, Alexander C Berg, Wan-Yen Lo, et al. Segment anything. *arXiv preprint arXiv:2304.02643*, 2023. [2](#), [3](#)
- [36] David M Knigge, David W Romero, Albert Gu, Efstratios Gavves, Erik J Bekkers, Jakub M Tomczak, Mark Hoogenboom, and Jan-Jakob Sonke. Modelling long range dependencies in nd: From task-specific to a general purpose cnn. *arXiv preprint arXiv:2301.10540*, 2023. [2](#), [8](#)
- [37] Victor Kulikov and Victor Lempitsky. Instance segmentation of biological images using harmonic embeddings. In *Proceedings of the IEEE/CVF Conference on Computer Vision and Pattern Recognition (CVPR)*, 2020. [2](#)
- [38] Kisuk Lee, Ran Lu, Kyle Luther, and H Sebastian Seung. Learning and segmenting dense voxel embeddings for 3d neuron reconstruction. *IEEE Transactions on Medical Imaging*, 40(12):3801–3811, 2021. [2](#)
- [39] T.C. Lee, R.L. Kashyap, and C.N. Chu. Building skeleton models via 3-d medial surface axis thinning algorithms. *CVGIP: Graphical Models and Image Processing*, 56(6): 462–478, 1994. [5](#)
- [40] Rui Li, Muye Zhu, Junning Li, Michael S Bienkowski, Nicholas N Foster, Hanpeng Xu, Tyler Ard, Ian Bowman, Changle Zhou, Matthew B Veldman, et al. Precise segmentation of densely interweaving neuron clusters using g-cut. *Nature communications*, 10(1):1549, 2019. [2](#)
- [41] Tsung-Yi Lin, Michael Maire, Serge J. Belongie, Lubomir D. Bourdev, Ross B. Girshick, James Hays, Pietro Perona, Deva Ramanan, Piotr Doll’ar, and C. Lawrence Zitnick. Microsoft COCO: common objects in context. *CoRR*, abs/1405.0312, 2014. [2](#)
- [42] Drew Linsley, Junkyung Kim, Vijay Veerabadrán, Charles Windolf, and Thomas Serre. Learning long-range spatial dependencies with horizontal gated recurrent units. In *Advances in Neural Information Processing Systems*. Curran Associates, Inc., 2018. [2](#)
- [43] Jean Livet, Family A. Weissman, Hyuno Kang, Ryan W. Draft, Ju Lu, Robyn A. Bennis, Joshua R. Sanes, and Jeff W. Lichtman. Transgenic strategies for combinatorial expression of fluorescent proteins in the nervous system. *Nature*, 450(7166):56–62, 2007. [19](#)
- [44] Xingzheng Lyu, Li Cheng, and Sanyuan Zhang. The retina benchmark for retinal vascular tree analysis. *Scientific Data*, 9(1):397, 2022. [2](#)
- [45] Matteo Maggioni, Vladimir Katkovnik, Karen Egiazarian, and Alessandro Foi. Nonlocal transform-domain filter for volumetric data denoising and reconstruction. *IEEE Transactions on Image Processing*, 22(1):119–133, 2013. [19](#)
- [46] Lena Maier-Hein, Annika Reinke, Patrick Godau, Minu D. Tizabi, Florian Büttner, Evangelia Christodoulou, Ben Glocker, Fabian Isensee, Jens Kleesiek, Michal Kozubek, Mauricio Reyes, Michael A. Riegler, Manuel Wiesenfath, Emre Kavur, Carole H. Sudre, Michael Baumgartner, Matthias Eisenmann, Doreen Heckmann-Nötzel, A. Tim Rädtsch, Laura Acion, Michela Antonelli, Tal Arbel, Spyridon Bakas, Arriel Benis, Matthew Blaschko, M. Jorge Cardoso, Veronika Cheplygina, Beth A. Cimini, Gary S. Collins,

- Keyvan Farahani, Luciana Ferrer, Adrian Galdran, Bram van Ginneken, Robert Haase, Daniel A. Hashimoto, Michael M. Hoffman, Merel Huisman, Pierre Jannin, Charles E. Kahn, Dagmar Kainmueller, Bernhard Kainz, Alexandros Karar-gyris, Alan Karthikesalingam, Hannes Kenngott, Florian Kofler, Annette Kopp-Schneider, Anna Kreshuk, Tahsin Kurc, Bennett A. Landman, Geert Litjens, Amin Madani, Klaus Maier-Hein, Anne L. Martel, Peter Mattson, Erik Meijering, Bjoern Menze, Karel G. M. Moons, Henning Müller, Brennan Nichyporuk, Felix Nickel, Jens Petersen, Nasir Rajpoot, Nicola Rieke, Julio Saez-Rodriguez, Clara I. Sánchez, Shravya Shetty, Maarten van Smeden, Ronald M. Summers, Abdel A. Taha, Aleksei Tiulpin, Sotirios A. Tsafaris, Ben Van Calster, Gaël Varoquaux, and Paul F. Jäger. Metrics reloaded: Pitfalls and recommendations for image analysis validation, 2022. [2](#), [4](#), [5](#)
- [47] Lisa Mais, Peter Hirsch, and Dagmar Kainmueller. Patch-perpix for instance segmentation. In *Computer Vision – ECCV 2020: 16th European Conference, Glasgow, UK, August 23–28, 2020, Proceedings, Part XXV*, page 288–304, Berlin, Heidelberg, 2020. Springer-Verlag. [2](#), [3](#), [7](#), [8](#), [16](#), [19](#)
- [48] Lisa Mais, Peter Hirsch, Claire Managan, Kaiyu Wang, Konrad Rokicki, Robert R Svirskas, Barry J Dickson, Wyatt Korff, Gerald M Rubin, Gudrun Ihrke, et al. Patchperpixmatch for automated 3d search of neuronal morphologies in light microscopy. *bioRxiv*, pages 2021–07, 2021. [16](#)
- [49] Linus Manubens-Gil, Zhi Zhou, Hanbo Chen, Arvind Ramanathan, Xiaoxiao Liu, Yufeng Liu, Alessandro Bria, Todd Gillette, Zongcai Ruan, Jian Yang, et al. Bigneuron: a resource to benchmark and predict performance of algorithms for automated tracing of neurons in light microscopy datasets. *Nature Methods*, pages 1–12, 2023. [2](#)
- [50] Pavel Matula, Martin Maška, Dmitry V. Sorokin, Petr Matula, Carlos Ortiz-de Solórzano, and Michal Kozubek. Cell tracking accuracy measurement based on comparison of acyclic oriented graphs. *PLOS ONE*, 10(12):1–19, 2015. [4](#), [5](#)
- [51] Geoffrey W Meissner, Aljoscha Nern, Zachary Dorman, Gina M DePasquale, Kaitlyn Forster, Theresa Gibney, Joanna H Hausenfluck, Yisheng He, Nirmala A Iyer, Jennifer Jeter, Lauren Johnson, Rebecca M Johnston, Kelley Lee, Brian Melton, Brianna Yarbrough, Christopher T Zuges, Jody Clements, Cristian Goina, Hideo Otsuna, Konrad Rokicki, Robert R Svirskas, Yoshinori Aso, Gwyneth M Card, Barry J Dickson, Erica Ehrhardt, Jens Goldammer, Masayoshi Ito, Dagmar Kainmueller, Wyatt Korff, Lisa Mais, Ryo Minegishi, Shigehiro Namiki, Gerald M Rubin, Gabriella R Sterne, Tanya Wolff, Oz Malkesman, and FlyLight Project Team. A searchable image resource of *Drosophila gal4* driver expression patterns with single neuron resolution. *eLife*, 12:e80660, 2023. [2](#), [3](#), [13](#), [14](#), [15](#), [16](#), [21](#)
- [52] Mai M Morimoto, Aljoscha Nern, Arthur Zhao, Edward M Rogers, Allan M Wong, Mathew D Isaacson, Davi D Bock, Gerald M Rubin, and Michael B Reiser. Spatial readout of visual looming in the central brain of *Drosophila*. *eLife*, 9:e57685, 2020. [21](#)
- [53] napari contributors. napari: a multi-dimensional image viewer for python, 2019. [17](#)
- [54] Aljoscha Nern, Barret D. Pfeiffer, and Gerald M. Rubin. Optimized tools for multicolor stochastic labeling reveal diverse stereotyped cell arrangements in the fly visual system. *Proceedings of the National Academy of Sciences*, 112(22):E2967–E2976, 2015. [3](#), [13](#)
- [55] Eric Nguyen, Karan Goel, Albert Gu, Gordon Downs, Preeti Shah, Tri Dao, Stephen Baccus, and Christopher Ré. S4nd: Modeling images and videos as multidimensional signals with state spaces. In *Advances in Neural Information Processing Systems*, 2022. [2](#), [8](#)
- [56] Adam Paszke, Sam Gross, Francisco Massa, Adam Lerer, James Bradbury, Gregory Chanan, Trevor Killeen, Zeming Lin, Natalia Gimelshein, Luca Antiga, Alban Desmaison, Andreas Kopf, Edward Yang, Zachary DeVito, Martin Raison, Alykhan Tejani, Sasank Chilamkurthy, Benoit Steiner, Lu Fang, Junjie Bai, and Soumith Chintala. PyTorch: An Imperative Style, High-Performance Deep Learning Library. In *Advances in Neural Information Processing Systems 32*, pages 8024–8035. Curran Associates, Inc., 2019. [19](#)
- [57] Hanchuan Peng, Michael Hawrylycz, Jane Roskams, Sean Hill, Nelson Spruston, Erik Meijering, and Giorgio A Ascoli. BigNeuron: Large-Scale 3D neuron reconstruction from optical microscopy images. *Neuron*, 87(2):252–256, 2015. [2](#)
- [58] Barret D Pfeiffer, Teri-T B Ngo, Karen L Hibbard, Christine Murphy, Arnim Jenett, James W Truman, and Gerald M Rubin. Refinement of tools for targeted gene expression in drosophila. *Genetics*, 186(2):735–755, 2010. [21](#)
- [59] Tingwei Quan, Hang Zhou, Jing Li, Sw Li, Anan Li, Yuxin Li, Xiaohua Lv, Qingming Luo, Hui Gong, and Shaoqun Zeng. Neurogps-tree: Automatic reconstruction of large-scale neuronal populations with dense neurites. *Nature Methods*, 13, 2015. [2](#)
- [60] Konrad Rokicki, Christopher M. Bruns, Cristian Goina, David Schauder, Donald J. Olbris, Eric T. Trautman, Rob Svirskas, Jody Clements, David Ackerman, Antje Kazimiers, Leslie L. Foster, Tom Dolafi, Mark Bolstad, Hideo Otsuna, Yang Yu, Todd Safford, and Sean D. Murphy. Janelia Workstation Codebase, 2019. [16](#)
- [61] Olaf Ronneberger, Philipp Fischer, and Thomas Brox. U-net: Convolutional networks for biomedical image segmentation. In *Medical Image Computing and Computer-Assisted Intervention–MICCAI 2015: 18th International Conference, Munich, Germany, October 5–9, 2015, Proceedings, Part III 18*, pages 234–241. Springer, 2015. [19](#)
- [62] Douglas H Roossien, Benjamin V Sadis, Yan Yan, John M Webb, Lia Y Min, Aslan S Dizaji, Luke J Bogart, Cristina Mazuski, Robert S Huth, Johanna S Stecher, Sriakhila Akula, Fred Shen, Ye Li, Tingxin Xiao, Madeleine Vandenbrink, Jeff W Lichtman, Takao K Hensch, Erik D Herzog, and Dawen Cai. Multispectral tracing in densely labeled mouse brain with nTracer. *Bioinformatics*, 35(18):3544–3546, 2019. [2](#)
- [63] Louis K Scheffer, C Shan Xu, Michal Januszewski, Zhiyuan Lu, Shin-ya Takemura, Kenneth J Hayworth, Gary B Huang, Kazunori Shinomiya, Jeremy Maitlin-Shepard, Stuart Berg,

- et al. A connectome and analysis of the adult drosophila central brain. *Elife*, 9:e57443, 2020. 16
- [64] Suprosanna Shit, Johannes C. Paetzold, Anjany Sekuboyina, Ivan Ezhov, Alexander Unger, Andrey Zhylyka, Josien P. W. Pluim, Ulrich Bauer, and Bjoern H. Menze. cldice - a novel topology-preserving loss function for tubular structure segmentation. In *Proceedings of the IEEE/CVF Conference on Computer Vision and Pattern Recognition (CVPR)*, pages 16560–16569, 2021. 2, 5
- [65] Janelia Scientific Computing Software. VVDViewer, 2019. open-source software funded by NIH grant R01-GM098151-01NIH grant R01-GM098151-01, <https://github.com/JaneliaSciComp/VVDViewer>. 4
- [66] J. Staal, M.D. Abramoff, M. Niemeijer, M.A. Viergever, and B. van Ginneken. Ridge-based vessel segmentation in color images of the retina. *IEEE Transactions on Medical Imaging*, 23(4):501–509, 2004. 2
- [67] Carsen Stringer, Tim Wang, Michalis Michaelos, and Marius Pachitariu. Cellpose: a generalist algorithm for cellular segmentation. *Nature Methods*, 18(1):100–106, 2021. 2
- [68] Uygur Sümbül, Douglas Roossien, Dawen Cai, Fei Chen, Nicholas Barry, John P Cunningham, Edward Boyden, and Liam Paninski. Automated scalable segmentation of neurons from multispectral images. In *Advances in Neural Information Processing Systems*. Curran Associates, Inc., 2016. 2, 7, 19
- [69] Yi Tay, Mostafa Dehghani, Samira Abnar, Yikang Shen, Dara Bahri, Philip Pham, Jinfeng Rao, Liu Yang, Sebastian Ruder, and Donald Metzler. Long range arena: A benchmark for efficient transformers. *CoRR*, abs/2011.04006, 2020. 2
- [70] Srinivas C. Turaga, Kevin L. Briggman, Moritz Helmstaedter, Winfried Denk, and H. Sebastian Seung. Maximin affinity learning of image segmentation. *CoRR*, 2009. 2
- [71] Fei Wang, Kaiyu Wang, Nora Forknall, Christopher Patrick, Tansy Yang, Ruchi Parekh, Davi Bock, and Barry J. Dickson. Neural circuitry linking mating and egg laying in drosophila females. *Nature*, 579(7797):101–105, 2020. 21
- [72] Donglai Wei, Kisuk Lee, Hanyu Li, Ran Lu, J. Alexander Bae, Zequan Liu, Lifu Zhang, Márcia dos Santos, Zudi Lin, Thomas Uram, Xueying Wang, Ignacio Arganda-Carreras, Brian Matejek, Narayanan Kasthuri, Jeff Lichtman, and Hanspeter Pfister. Axonem dataset: 3d axon instance segmentation of brain cortical regions. In *Medical Image Computing and Computer Assisted Intervention – MICCAI 2021*, pages 175–185, Cham, 2021. Springer International Publishing. 2, 3
- [73] Martin Weigert, Uwe Schmidt, Robert Haase, Ko Sugawara, and Gene Myers. Star-convex polyhedra for 3d object detection and segmentation in microscopy. In *Proceedings of the IEEE/CVF Winter Conference on Applications of Computer Vision (WACV)*, 2020. 2
- [74] Johan Winnubst, Erhan Bas, Tiago A. Ferreira, Zhuhao Wu, Michael N. Economou, Patrick Edson, Ben J. Arthur, Christopher Bruns, Konrad Rokicki, David Schauder, Donald J. Olbris, Sean D. Murphy, David G. Ackerman, Cameron Arshadi, Perry Baldwin, Regina Blake, Ahmad Elsayed, Mashura Hasan, Daniel Ramirez, Bruno Dos Santos, Monet Weldon, Amina Zafar, Joshua T. Dudman, Charles R. Gerfen, Adam W. Hantman, Wyatt Korff, Scott M. Sternson, Nelson Spruston, Karel Svoboda, and Jayaram Chandrashekar. Reconstruction of 1,000 projection neurons reveals new cell types and organization of long-range connectivity in the mouse brain. *Cell*, 179(1):268–281.e13, 2019. 2
- [75] Steffen Wolf, Constantin Pape, Alberto Bailoni, Nasim Rahaman, Anna Kreshuk, Ullrich Köthe, and Fred A. Hamprecht. The mutex watershed: Efficient, parameter-free image partitioning. In *ECCV (4)*, pages 571–587. Springer, 2018. 2
- [76] Yang Yu and Hanchuan Peng. Automated high speed stitching of large 3d microscopic images. In *2011 IEEE International Symposium on Biomedical Imaging: From Nano to Macro*, pages 238–241, 2011. 16
- [77] Bolei Zhou, Hang Zhao, Xavier Puig, Sanja Fidler, Adela Barriuso, and Antonio Torralba. Scene parsing through ade20k dataset. In *2017 IEEE Conference on Computer Vision and Pattern Recognition (CVPR)*, pages 5122–5130, 2017. 2
- [78] Hang Zhou, Shiwei Li, Anan Li, Qing Huang, Feng Xiong, Ning Li, Jiacheng Han, Hongtao Kang, Yijun Chen, Yun Li, et al. Gtree: an open-source tool for dense reconstruction of brain-wide neuronal population. *Neuroinformatics*, 19:305–317, 2021. 2

FISBe: A real-world benchmark dataset for instance segmentation of long-range thin filamentous structures

Supplementary Material

A. Appendix

A.1. Dataset Documentation

A.1.1 Datasheet

In this section we answer the Datasheet for Datasets questionnaire [23] to document FISBe, the FlyLight Instance Segmentation Benchmark dataset. It contains information about motivation, composition, collection, preprocessing, usage, licensing as well as hosting and maintenance plan.

A.1.1.1 Motivation

For what purpose was the dataset created? Was there a specific task in mind? Was there a specific gap that needed to be filled? Please provide a description.

Segmenting individual neurons in multi-neuron light microscopy (LM) recordings is intricate due to the long, thin filamentous and widely branching morphology of individual neurons, the tight interweaving of multiple neurons, and LM-specific imaging characteristics like partial volume effects and uneven illumination. These properties reflect a current key challenge for deep-learning models across domains, namely to efficiently capture long-range dependencies in the data. While methodological research on this topic is buzzing in the machine learning community, to date, respective methods are typically benchmarked on synthetic datasets. To fill this gap, we created the FlyLight Instance Segmentation Benchmark dataset, to the best of our knowledge, the first publicly available multi-neuron LM dataset with pixel-wise ground truth and the first real-world benchmark dataset for instance segmentation of long thin filamentous objects.

Who created this dataset (e.g., which team, research group) and on behalf of which entity (e.g., company, institution, organization)?

This dataset was created in a collaboration of the Max-Delbrueck-Center for Molecular Medicine in the Helmholtz Association (MDC) and the Howard Hughes Medical Institute Janelia Research Campus. More precisely, the Kainmueller lab at the MDC and the Project Technical Resources Team at Janelia.

Who funded the creation of the dataset? If there is an associated grant, please provide the name of the grantor and the grant name and number.

Howard Hughes Medical Institute Janelia Research Campus and Max-Delbrueck-Center for Molecular Medicine in the Helmholtz Association (MDC) funded the creation of the dataset.

A.1.1.2 Composition

What do the samples³ that comprise the dataset represent (e.g., documents, photos, people, countries)? Are there multiple types of samples (e.g., movies, users, and ratings; people and interactions between them; nodes and edges)? Please provide a description.

The dataset consists of 3d multi-neuron multicolor light microscopy images and their respective pixel-wise instance segmentation masks. The "raw" light microscopy data shows neurons of the fruit fly *Drosophila Melanogaster* acquired with a technique called MultiColor FlpOut (MCFO) [51, 54]. Fruit fly brains of different transgenic lines (e.g.

³We changed *instances* to *samples* when referring to images of the dataset to not use the term ambiguously; instead we only use *instances* to refer to *object instances* in images.

GAL4 lines [31]) were imaged, each transgenic line tags a different set of neurons. There are multiple MCFO images of the same transgenic line, where each MCFO image expresses (shows) a stochastic subset of the tagged neurons. The neurons contained in each image were manually annotated by trained expert annotators. The dataset is split into a *completely* labeled (all neurons in the image are manually segmented) and a *partly* labeled (a subset of neurons in the image is manually segmented) set.

How many samples/instances are there in total (of each type, if appropriate)?

The *completely* labeled set comprises 30 images with 139 labeled neurons in total, and the *partly* labeled set comprises 71 images with 451 labeled neurons in total.

Does the dataset contain all possible samples or is it a subset (not necessarily random) of samples from a larger set? If the dataset is a sample, then what is the larger set? Is the sample representative of the larger set (e.g., geographic coverage)? If so, please describe how this representativeness was validated/verified. If it is not representative of the larger set, please describe why not (e.g., to cover a more diverse range of instances, because instances were withheld or unavailable).

The dataset contains a subset of 101 images from the "40x Gen1" set of [51]. The full "40x Gen1" set consists of 46,791 images of 4575 different transgenic lines. From this set, we selected relatively sparse images in terms of number of expressed neurons which seemed feasible for manual annotation. Thus, our dataset is not representative for the full "40x Gen1" MCFO collection.

What data does each sample consist of? "Raw" data (e.g., unprocessed text or images) or features? Is there a label or target associated with each sample? Please provide a description.

Each sample consists of a single 3d MCFO image of neurons of the fruit fly. For each image, we provide a pixel-wise instance segmentation for all separable neurons. Each sample is stored as a separate *zarr* file ("Zarr is a file storage format for chunked, compressed, N-dimensional arrays based on an open-source specification." <https://zarr.readthedocs.io>). The image data ("raw") and the segmentation ("gt_instances") are stored as two arrays within a single *zarr* file. The segmentation mask for each neuron is stored in a separate channel. The order of dimensions is CZYX. In Python the data can, for instance, be opened with:

```
import zarr
raw = zarr.open(
    <path_to_zarr>,
    path="volumes/raw")
seg = zarr.open(
    <path_to_zarr>,
    path="volumes/gt_instances")
```

Zarr arrays are read lazily on-demand. Many functions that expect numpy arrays also work with zarr arrays. The arrays can also explicitly be converted to numpy arrays with:

```
import numpy as np
raw_np = np.array(raw)
```

Is any information missing from individual samples? If so, please provide a description, explaining why this information is missing (e.g., because it was unavailable). This does not include intentionally removed information, but might include, e.g., redacted text.

Not all neuronal structures could be segmented within all images of the provided dataset. Mainly, there are two reasons: (1) there are overlapping neurons with the same or a similar color that could not be separated due to the partial volume effect, and (2) some neuronal structures cannot be delineated correctly in the presence of noisy background in the same color as the neuron itself. In the *completely* labeled set all neuronal structures have been segmented, in the *partly* labeled set some structures are missing.

Are relationships between individual samples made explicit (e.g., users' movie ratings, social network links)? If so, please describe how these relationships are made explicit.

Yes, one transgenic line is often imaged multiple times as only a stochastic subset of all tagged neurons is visible per MCFO image. Moreover, the same neuron might be tagged in multiple transgenic lines.

Are there recommended data splits (e.g., training, development/validation, testing)? If so, please provide a description of these splits, explaining the rationale behind them.

Yes, we provide a recommended data split for training, validation and testing. The files in the provided download are presorted according to this recommendation. When splitting the data into sets, we made sure that images of the same transgenic lines are in the same split and paid attention to having similar proportions of images with overlapping neurons as well as having a similar average number of neurons per image in each split.

Are there any errors, sources of noise, or redundancies in the dataset? If so, please provide a description.

There might be uneven illumination resulting in gaps within neurons in the raw microscopy images as well as the corre-

sponding annotations. This is intrinsic to this kind of light microscopy images.

Is the dataset self-contained, or does it link to or otherwise rely on external resources (e.g., websites, tweets, other datasets)? If it links to or relies on external resources, a) are there guarantees that they will exist, and remain constant, over time; b) are there official archival versions of the complete dataset (i.e., including the external resources as they existed at the time the dataset was created); c) are there any restrictions (e.g., licenses, fees) associated with any of the external resources that might apply to a future user? Please provide descriptions of all external resources and any restrictions associated with them, as well as links or other access points, as appropriate.

Yes, the dataset is self-contained. There is an external, additional source of raw images that could potentially be used for self-supervised learning. The raw images in our dataset are a subset of the released MCFO collection of the Fly-Light project [51]. The whole collection can be downloaded at <https://gen1mcfo.janelia.org>. Note though that there are no segmentation masks available for these images.

Does the dataset contain data that might be considered confidential (e.g., data that is protected by legal privilege or by doctor-patient confidentiality, data that includes the content of individuals non-public communications)? If so, please provide a description.

No.

A.1.1.3 Collection Process

How was the data associated with each sample acquired? Was the data directly observable (e.g., raw text, movie ratings), reported by subjects (e.g., survey responses), or indirectly inferred/derived from other data (e.g., part-of-speech tags, model-based guesses for age or language)? If data was reported by subjects or indirectly inferred/derived from other data, was the data validated/verified? If so, please describe how.

The content of the raw images was directly recorded using confocal microscopes. The annotations were created manually.

What mechanisms or procedures were used to collect the data (e.g., hardware apparatus or sensor, manual human curation, software program, software API)? How were these mechanisms or procedures validated?

Imaging was performed using eight Zeiss LSM 710 or 780 laser scanning confocal microscopes (for more information on the imaging process see [51]). Two trained expert annotators manually segmented and proof-read each other to segment the neurons in these im-

ages using the interactive rendering tool VVD Viewer (<https://github.com/JaneliaSciComp/VVDViewer>).

If the dataset is a sample from a larger set, what was the sampling strategy (e.g., deterministic, probabilistic with specific sampling probabilities)?

We manually selected images from the larger "40x Gen1" collection. We chose images that contained a sparse set of neurons and that contained neurons that preferably were not contained in previously selected images.

Who was involved in the data collection process (e.g., students, crowdworkers, contractors) and how were they compensated (e.g., how much were crowdworkers paid)?

The data collection process was done by full time employees at the Howard Hughes Medical Institute Janelia Research Campus and the Max-Delbrueck-Center for Molecular Medicine in the Helmholtz Association (MDC).

Over what timeframe was the data collected? Does this timeframe match the creation timeframe of the data associated with the samples (e.g., recent crawl of old news articles)? If not, please describe the timeframe in which the data associated with the samples was created.

MCFO selection and manual annotation were mainly done in 2018 and 2019. The respective acquisition date of the MCFO sample is noted within the sample name in "YYYYMMDD" format. Most samples of our dataset were acquired in 2017 and 2018.

Were any ethical review processes conducted (e.g., by an institutional review board)? If so, please provide a description of these review processes, including the outcomes, as well as a link or other access point to any supporting documentation.

There was no ethical review process conducted as we did not record any new animal data, the dataset does not relate to people and it does not contain confidential data.

Does the dataset relate to people? If not, you may skip the remaining questions in this section.

No.

A.1.1.4 Preprocessing/cleaning/labeling

Was any preprocessing/cleaning/labeling of the data done (e.g., discretization or bucketing, tokenization, part-of-speech tagging, SIFT feature extraction, removal of instances, processing of missing values)? If so, please provide a description. If not, you may skip the remainder of the questions in this section.

The following preprocessing was done for each image: The central brain and part of the ventral nerve cord (VNC) were

recorded in tiles by the light microscope. The tiles were stitched together and distortion corrected (for more information see [76]).

Was the “raw” data saved in addition to the preprocessed/cleaned/labeled data (e.g., to support unanticipated future uses)? If so, please provide a link or other access point to the “raw” data.

The original images are available at <https://gen1mcfo.janelia.org>.

Is the software used to preprocess/clean/label the samples available? If so, please provide a link or other access point.

The image processing, such as distortion correction and stitching, is done by using the open-source software Janelia Workstation [60].

A.1.1.5 Uses

Has the dataset been used for any tasks already? If so, please provide a description.

In [47], an earlier, unpublished version of our dataset has been used to qualitatively evaluate PatchPerPix, a deep learning-based instance segmentation method. The trained model was then applied to ~40.000 samples of the MCFO collection [48, 51] to search for given neuronal structures extracted from electron microscopy (EM) data [63]. PatchPerPix is also used as one of three baselines to showcase this published version of our dataset.

Is there a repository that links to any or all papers or systems that use the dataset? If so, please provide a link or other access point.

As they are getting published, we will reference them at <https://kainmueller-lab.github.io/fisbe>

What (other) tasks could the dataset be used for?

The dataset can be used for a wide range of method development tasks such as capturing long-range dependencies, segmentation of thin filamentous structures, self- and semi-supervised training or denoising. Advances in these areas can in turn facilitate scientific discoveries in basic neuroscience by providing improved neuron reconstructions for morphological and functional analyses.

A.1.1.6 Distribution

Will the dataset be distributed to third parties outside of the entity (e.g., company, institution, organization) on behalf of which the dataset was created? If so, please provide a description.

The dataset will be publicly available.

How will the dataset be distributed (e.g., tarball on website, API, GitHub) Does the dataset have a digital object identifier (DOI)?

The dataset will be distributed through [zenodo](https://zenodo.org/doi/10.5281/zenodo.10875063) (DOI: 10.5281/zenodo.10875063) and our project page <https://kainmueller-lab.github.io/fisbe>.

When will the dataset be distributed?

With publication of the accompanying paper.

Will the dataset be distributed under a copyright or other intellectual property (IP) license, and/or under applicable terms of use (ToU)? If so, please describe this license and/or ToU, and provide a link or other access point to, or otherwise reproduce, any relevant licensing terms or ToU, as well as any fees associated with these restrictions.

The dataset will be distributed under the Creative Commons Attribution 4.0 International (CC BY 4.0) license (<https://creativecommons.org/licenses/by/4.0/>).

Have any third parties imposed IP-based or other restrictions on the data associated with the samples? If so, please describe these restrictions, and provide a link or other access point to, or otherwise reproduce, any relevant licensing terms, as well as any fees associated with these restrictions.

All MCFO images have previously been made publicly available by [51] under the same license (CC BY 4.0) at <https://gen1mcfo.janelia.org>.

A.1.1.7 Maintenance

Who will be supporting/hosting/maintaining the dataset?

Lisa Mais supports and maintains the dataset.

How can the owner/curator/manager of the dataset be contacted (e.g., email address)?

Lisa Mais and Dagmar Kainmueller can be contacted at {firstname.lastname}@mdc-berlin.de.

Is there an erratum? If so, please provide a link or other access point.

Errata will be published at <https://kainmueller-lab.github.io/fisbe>.

Will the dataset be updated (e.g., to correct labeling errors, add new samples, delete samples)? If so, please describe how often, by whom, and how updates will be communicated to users (e.g., mailing list, GitHub)?

The dataset will be updated to correct erroneous segmentation and potentially to add new samples and annotations. It will be updated when a relevant number of updates has accumulated. Updates will be communicated through <https://kainmueller-lab.github.io/fisbe>.

Will older versions of the dataset continue to be supported/hosted/maintained? If so, please describe how. If not, please describe how its obsolescence will be communicated to users.

We publish our dataset on zenodo. Zenodo supports versioning, including DOI versioning. Older versions of the dataset will thus stay available.

If others want to extend/augment/build on/contribute to the dataset, is there a mechanism for them to do so? If so, please provide a description. Will these contributions be validated/verified? If so, please describe how. If not, why not? Is there a process for communicating/distributing these contributions to other users? If so, please provide a description.

We welcome contributions to our dataset. Errata, new samples and annotations and other contributions can be contributed via *github issues* at <https://kainmueller-lab.github.io/fisbe>. We will verify such contributions and update the dataset accordingly.

A.1.2 How to Open and View Image Files

We recommend viewing the FISBe dataset with napari [53]. The following instructions have been tested with Linux. While they should also work for Windows and MacOS, they might require some small changes. Please follow the official installation instructions (<https://napari.org/stable/>):

```
conda create -y -n napari-env -c \
conda-forge python=3.9
conda activate napari-env
pip install "napari[all]" zarr
```

Then save the following Python script (also included in the provided download of our dataset):

```
import zarr, sys, napari

raw = zarr.load(
    sys.argv[1], path="volumes/raw")
gt = zarr.load(
    sys.argv[1], path="volumes/gt_instances")

viewer = napari.Viewer(ndisplay=3)
for idx, gt in enumerate(gts):
    viewer.add_labels(
        gt, rendering='translucent',
        blending='additive', name=f'gt_{idx}')
)

viewer.add_image(raw[0], colormap="red",
    name='raw_r', blending='additive')
viewer.add_image(raw[1], colormap="green",
    name='raw_g', blending='additive')
viewer.add_image(raw[2], colormap="blue",
    name='raw_b', blending='additive')
napari.run()
```

Execute it from the command line to view the image:

```
python <script_name.py> <path-to-file>/
R9F03-20181030_62_B5.zarr
```

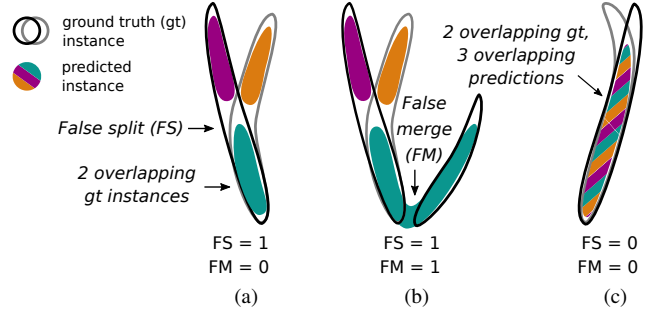


Figure 5. Exemplary challenges for many-to-many matching with overlaps. (a) One predicted instance lies completely within an overlapping gt region, but it should only be assigned to one of them; (b) one predicted instance covers one gt and merges with an overlapping gt region, here it should be assigned to the single gt and one of the overlapping ones; and (c) three overlapping predicted instances cover two overlapping gt instances, here only two predicted instances should be matched to the two gt instances respectively (the other predicted instance should rather only count as false positive than as false split). As there are plenty of scenarios how gt and predicted instances can overlap, special treatment for overlapping regions is difficult and error-prone. However, our proposed algorithm (see Alg. 1 in the main paper) naturally handles such overlaps by keeping track of already matched pixels (as opposed to only on the level of instances).

A.2. Extended Metrics Information

Table 2 summarizes all used metrics with their localization criterion and matching. Fig. 5 highlights some of the challenges of computing a consistent many-to-many matching for overlapping instances. Fig. 6 visualizes and quantifies a comprehensive set of different edge cases of our evaluation metrics.

Table 2. Overview of localization criterion and matching algorithm for used scores. Last line shows cardinalities of the ground truth-to-prediction relationships.

Score	avF1	C	FS	FM	cIDice _{TP}
Loc.	cIDice	cIPrec.	cIRecall	cIRecall	cIDice
Match.	greedy	greedy	greedy	greedy	greedy
	1:1	1:n	n:m	n:m	1:1

A.3. Extended Baseline Information and Results

We describe our three baseline methods in the following sections, namely PatchPerPix in Sec. A.3.1, Flood Filling Networks in Sec. A.3.2 and Duan et al.’s color clustering in Sec. A.3.3. The evaluation code is available here: <https://github.com/Kainmueller-Lab/evaluate-instance-segmentation>. Please see Table 3 and 4 for the extended quantitative results. Qualitative results for all three

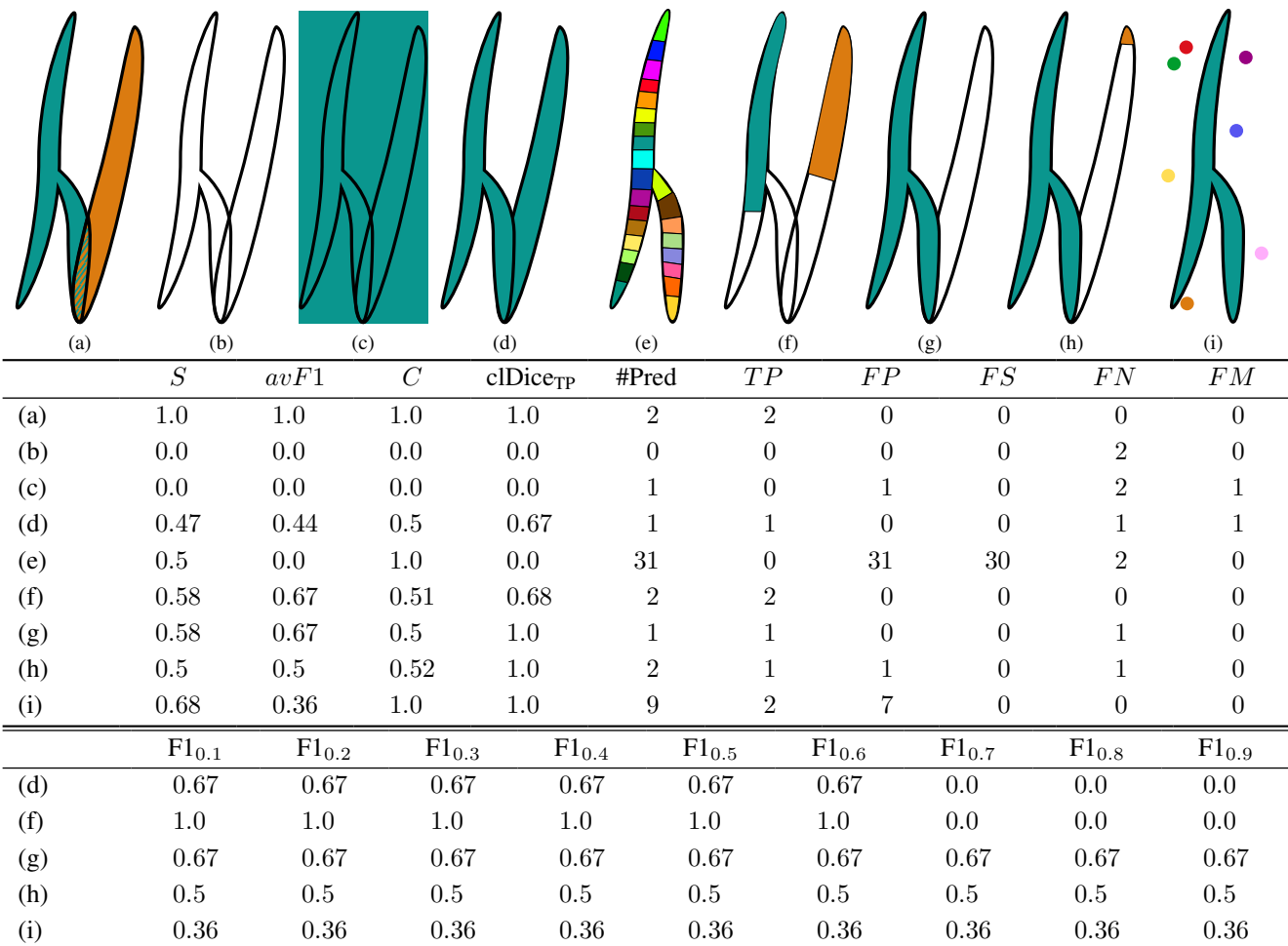


Figure 6. Quantitative assessment of a number of different edge cases of our evaluation metrics (outline: ground truth, color: predictions, $th = 0.5$), highlighting their applicability and validity for FISBe. In (a) we have a perfect prediction, the score is perfect and there are no errors. In (b) we have no prediction, the score is zero and we have as many FN as there are instances. In (c) we have one prediction that covers the whole image; as the $cIDice$ value is too low, there is no TP, so $avF1$ is still zero. When computing the $cIPrecision$ for the predicted instance, the corresponding skeleton will likely have the largest overlap with the ground truth background and will be matched to it. Thus, C will be zero as well. In (d) we have a perfect foreground segmentation but the two ground truth instances are merged; the predicted instance is assigned to one of the ground truth instances, resulting in $C = 0.5$. Assuming $cIDice = 0.67$ for the one match (and thus $cIDice_{TP} = 0.67$), we have $F1 = 0.67$ for $th < 0.7$ and 0 otherwise. In (e) we again have a perfect foreground segmentation but there are many small instances; $cIDice$ for each pair of predicted and ground truth instances is < 0.1 , thus $avF1 = 0$ and $cIDice_{TP} = 0$; however, $C = 1.0$ because both instances are completely covered (and multiple predicted instances can be matched to one ground truth instance). In (f), (g) and (h) overall slightly more than half of the total ground truth is covered; in (f) both instances are covered slightly more than half; in (g) one instance is covered completely and the other is not; in (h) one instance is covered completely and only a tiny part of the other; to distinguish the cases quantitatively, one has to look at the details: about the same amount of ground truth is covered, thus C has a similar value; in (f) $cIDice_{TP}$ is worst as both predicted instances are counted as TP, yet both only cover just over half of their respective ground truth instance; furthermore, while $avF1$ is identical for (f) and (g), when looking at the full range of $F1_{th}$ values there are more differences: in (f) there are 2 TP for $th < 0.7$, resulting in $F1$ being equal to 1 for smaller thresholds and equal to 0 for larger thresholds; in (g) there is 1 TP for the full range of thresholds, but also 1 FN; in both cases this results in $avF1 = 0.67$; finally in (h) there is 1 TP for the full range of thresholds, 1 FN as in (g), but also 1 FP, resulting in $avF1 = 0.5$. In (i) we have a perfect prediction as in (a), but in addition we have a number of small FP, due to noise categorized as foreground; the coverage values are not affected, but the $avF1$ value drops. One could argue that (h) should be better than (g) as more is detected; however, if a prediction is too small, it is, in general, more likely to be noise. One could also argue that (d) should be better than (g), as both neurons are detected, just merged; however, for downstream tasks having one fully correct instance that can directly be used is often more valuable than first having to manually fix errors.

baselines are shown in Fig. 7 and a visualization of typical error types for PatchPerPix is presented in Fig. 8.

A.3.1 PatchPerPix

We use PatchPerPix [47] with a 3-level 3d U-Net [9, 61] with 20 initial feature maps, tripled at each downsampling layer. The predicted patches are of size $7 \times 7 \times 7$ pixels. We use the base model without the additional patch decoder. In addition to the patches the model is trained to predict how many instances there are per pixel (*numinst* in the code) modelled as a categorical prediction task with the categories: zero, one and more than one instance. We use PyTorch [56] in combination with gunpowder [27] for training with the following standard random augmentations: Elastic, Intensity, Flipping. We add the following augmentations: Overlay (overlying two random image crops to simulate denser images), Permute (randomly permute color channels), Hue (random rotation of the color wheel). We train the model only on the completely labeled data as the training is not directly applicable to partly labeled data.

The models are trained for 300k iterations with a learning rate of 0.0001 using Adam[34], storing weight checkpoints every 10k iterations. We use a batch size of 2 and train on random crops. As most images are in large part background, we sample foreground and areas where neurons overlap with higher probability. The exact ratios depend on the model and are detailed in the respective provided configuration files. The training code is available here: <https://github.com/Kainmueller-Lab/PatchPerPix>.

We select the best checkpoint, the best patch threshold and the best threshold for the *numinst* prediction based on the validation set and report both the validation results and the final results on the test set (both combined and separately for the completely labeled and the partly labeled dataset). We observed that the models tend to overestimate the case of a single neuron in a given region and underestimate background and neuron overlaps. To counter this, instead of using a simple $\arg \max$, we additionally select an optimal threshold based on the validation results.

PatchPerPix can only handle overlaps up to the size of the patch size. As its instance assembly step is computationally demanding for 3d data, the currently applicable patch size is restricted. In order to be able to handle larger overlaps, PatchPerPix needs to be scaled up in future work.

A.3.2 Flood Filling Networks

For Flood Filling Networks (FFN) we mainly follow the proposed architecture from [29] and the publicly available code⁴. We use 12 stacked convolution modules with skip

⁴original code: <https://github.com/google/ffn>; and adapted for FISBe: <https://github.com/Kainmueller-Lab/ffn>

connections in between, where each convolution module consists of two 3d convolution layers. The field of view (FoV) size, which corresponds to the spatial dimensions of the network’s input and output size, is $33 \times 33 \times 33$ and we adapted the network to work with three input channel. FFNs move their current FoV by a short distance after each update to be able to trace the entire object. For this, we use the cuboid movement policy described in [30] with step size 8 for each dimension. We apply standard data augmentation by flipping and permuting spatial axis. We train the models for 2m iterations with batch size 4. The sampling strategy is the same as in the original work.

During training we use seeds (starting position of the FoV) generated from ground truth. For prediction we create the seeds as follows: We convert the three channel input to a grayscale volume and threshold it to obtain a foreground mask, where we filter out small connected components. Finally, we take local maxima on the corresponding distance transform map. We determine both thresholds (foreground and small connected components size) during validation. Aside from that, we choose the best checkpoint, the best FoV movement threshold and the best final segmentation threshold based on validation.

We train and test FFNs both on only the completely labeled dataset and on the full dataset. In contrast to PatchPerPix, FFNs only consider one instance at a time, which means that there are no changes necessary to train FFNs on partly labeled samples.

A.3.3 Color Clustering

Duan et al. [14] propose a non-learned color clustering algorithm based on [68] to segment mouse neurons in Brainbow [43] images. Brainbow is a stochastic labeling technique to image neurons in unique colors with light microscopy. This assumption does not hold for our FISBe dataset, where multiple neurons and abundant noise can be of the same color. Thus, some steps of the pipeline (denoising, supervoxel generation, color clustering, linkage bridging) need to be adapted to fit our dataset.⁵

Following the original work, we denoise our 3d images with bm4d [45]. We use $\sigma = 0.05$ as noise standard deviation, and normalize and denoise each channel separately. For supervoxel generation, we threshold the denoised image with foreground threshold $t_{fg} = 0.08$, apply distance transform, and run watershed transform with local maxima as seeds and the thresholded foreground as mask. All connected components smaller than threshold $t_{rm} = 800$ are removed. In the next step, all supervoxels are clustered with Gaussian Mixture Models (GMM). We create an adjacency matrix where supervoxel pairs have a value > 0 , if their spatial and color distance is smaller than certain thresholds

⁵code: <https://github.com/Kainmueller-Lab/brainbow>

Table 3. Quantitative results of our baseline models on the *combined*, *completely* and *partly* labeled FISBe datasets. We train models both only on the completely labeled data (ppp, FFN), and on the completely and the partly labeled data (FFN+partly). Note that the scores are not directly comparable to each other across datasets (combined, completely, partly), but they are comparable across splits (val, test) and methods within each dataset. We report mean and standard deviation (\pm) over three independent runs (except for Duan et al.’s as it is non-learned). For all scores except FS and FM higher values are better. Continued in Table 4.

Split	Method	S	$avF1$	C	$clDice_{TP}$	FS	FM	C_{dim}	C_{ovlp}	tp	tp_{dim}	tp_{ovlp}
Combined												
Val	ppp	0.38 \pm 0.02	0.41 \pm 0.02	0.35 \pm 0.01	0.75 \pm 0.02	6.0 \pm 0.8	24 \pm 1.6	0.12 \pm 0.01	0.38 \pm 0.04	0.46 \pm 0.01	0.16 \pm 0.04	0.39 \pm 0.03
	FFN	0.25 \pm 0.01	0.27 \pm 0.01	0.23 \pm 0.01	0.79 \pm 0.01	7.0 \pm 2.9	12 \pm 2.0	0.03 \pm 0.01	0.30 \pm 0.01	0.32 \pm 0.01	0.04 \pm 0.01	0.37 \pm 0.02
	FFN+partly	0.27 \pm 0.01	0.29 \pm 0.01	0.24 \pm 0.01	0.79 \pm 0.01	7.7 \pm 2.6	14 \pm 0.8	0.02 \pm 0.01	0.33 \pm 0.02	0.34 \pm 0.03	0.03 \pm 0.00	0.38 \pm 0.04
	Duan et al.	0.24	0.26	0.22	0.70	14	13	0.02	0.28	0.37	0.03	0.42
Test	ppp	0.35 \pm 0.00	0.34 \pm 0.01	0.35 \pm 0.01	0.80 \pm 0.00	19 \pm 2.9	52 \pm 3.4	0.16 \pm 0.03	0.27 \pm 0.04	0.36 \pm 0.01	0.19 \pm 0.04	0.19 \pm 0.03
	FFN	0.25 \pm 0.03	0.22 \pm 0.04	0.29 \pm 0.02	0.80 \pm 0.01	17 \pm 1.7	39 \pm 5.3	0.03 \pm 0.01	0.26 \pm 0.03	0.32 \pm 0.03	0.00 \pm 0.00	0.24 \pm 0.05
	FFN+partly	0.27 \pm 0.01	0.24 \pm 0.02	0.31 \pm 0.00	0.80 \pm 0.01	18 \pm 3.7	36 \pm 3.6	0.04 \pm 0.01	0.28 \pm 0.01	0.36 \pm 0.01	0.03 \pm 0.00	0.28 \pm 0.01
	Duan et al.	0.30	0.27	0.33	0.77	45	29	0.03	0.36	0.37	0.03	0.34
Completely												
Val	ppp	0.30 \pm 0.03	0.34 \pm 0.04	0.27 \pm 0.03	0.72 \pm 0.02	1.7 \pm 1.7	3.7 \pm 1.3	0.07 \pm 0.01	0.41 \pm 0.07	0.37 \pm 0.06	0.06 \pm 0.04	0.47 \pm 0.12
	FFN	0.18 \pm 0.01	0.21 \pm 0.01	0.15 \pm 0.02	0.78 \pm 0.02	0.3 \pm 0.5	0.0 \pm 0.0	0.10 \pm 0.00	0.28 \pm 0.02	0.21 \pm 0.02	0.00 \pm 0.00	0.40 \pm 0.00
	FFN+partly	0.20 \pm 0.01	0.24 \pm 0.02	0.17 \pm 0.00	0.81 \pm 0.02	0.7 \pm 0.5	0.3 \pm 0.5	0.00 \pm 0.00	0.32 \pm 0.01	0.22 \pm 0.02	0.00 \pm 0.00	0.40 \pm 0.00
	Duan et al.	0.16	0.17	0.15	0.65	2	1	0.00	0.25	0.24	0.00	0.40
Test	ppp	0.34 \pm 0.02	0.29 \pm 0.04	0.40 \pm 0.02	0.81 \pm 0.02	3.0 \pm 0.8	4.3 \pm 1.3	0.14 \pm 0.05	0.42 \pm 0.03	0.45 \pm 0.01	0.19 \pm 0.09	0.38 \pm 0.10
	FFN	0.18 \pm 0.04	0.11 \pm 0.08	0.26 \pm 0.01	0.77 \pm 0.05	2.0 \pm 0.8	2.0 \pm 1.4	0.02 \pm 0.02	0.24 \pm 0.03	0.31 \pm 0.06	0.00 \pm 0.00	0.25 \pm 0.10
	FFN+partly	0.19 \pm 0.02	0.10 \pm 0.03	0.29 \pm 0.02	0.80 \pm 0.01	2.3 \pm 0.5	1.7 \pm 0.5	0.03 \pm 0.01	0.32 \pm 0.04	0.34 \pm 0.06	0.02 \pm 0.03	0.42 \pm 0.12
	Duan et al.	0.28	0.23	0.33	0.81	6	1	0.02	0.43	0.38	0.00	0.50
Partly												
Val	ppp	0.48 \pm 0.00	0.52 \pm 0.00	0.45 \pm 0.01	0.79 \pm 0.00	3.7 \pm 0.9	20 \pm 0.0	0.19 \pm 0.01	0.35 \pm 0.01	0.51 \pm 0.0	0.25 \pm 0.02	0.37 \pm 0.00
	FFN	0.34 \pm 0.01	0.36 \pm 0.01	0.32 \pm 0.01	0.79 \pm 0.01	7.3 \pm 2.9	12 \pm 1.6	0.06 \pm 0.02	0.33 \pm 0.00	0.37 \pm 0.02	0.06 \pm 0.02	0.39 \pm 0.03
	FFN+partly	0.34 \pm 0.02	0.36 \pm 0.03	0.32 \pm 0.01	0.77 \pm 0.01	8.0 \pm 1.6	13 \pm 0.9	0.04 \pm 0.02	0.34 \pm 0.02	0.38 \pm 0.03	0.03 \pm 0.02	0.39 \pm 0.04
	Duan et al.	0.32	0.35	0.30	0.74	12	12	0.04	0.31	0.41	0.04	0.43
Test	ppp	0.35 \pm 0.01	0.40 \pm 0.00	0.31 \pm 0.02	0.79 \pm 0.01	15 \pm 1.9	46 \pm 1.7	0.15 \pm 0.02	0.15 \pm 0.02	0.33 \pm 0.01	0.13 \pm 0.02	0.17 \pm 0.02
	FFN	0.33 \pm 0.02	0.35 \pm 0.02	0.32 \pm 0.02	0.80 \pm 0.01	16 \pm 2.5	37 \pm 4.0	0.03 \pm 0.01	0.23 \pm 0.03	0.34 \pm 0.02	0.00 \pm 0.00	0.23 \pm 0.04
	FFN+partly	0.34 \pm 0.02	0.36 \pm 0.03	0.33 \pm 0.02	0.82 \pm 0.01	17 \pm 2.5	35 \pm 3.7	0.04 \pm 0.01	0.25 \pm 0.03	0.34 \pm 0.02	0.05 \pm 0.00	0.25 \pm 0.01
	Duan et al.	0.33	0.32	0.34	0.73	39	28	0.04	0.28	0.37	0.05	0.32

($\delta_s = 5$, $\delta_c = 14$). Moreover, we use the Bayes Information Criterion (BIC) to determine the number of clusters for the GMM clustering. Finally, as same colored, but not touching neurons are clustered together, we apply connected component analysis for each GMM cluster with a distance threshold ($\Delta_s = 20$). Please note, that differing from the original works, we omit supervoxel subdivision and merging, PCA as well as linking bridging, because these steps did not im-

prove performance for our dataset. We determined σ , t_{fg} , t_{rm} , δ_s , δ_c and Δ_s during validation.

A.4. Biological Background and Motivation

This section gives a brief overview of the advances our dataset will facilitate in the field of basic neuroscience. Based on neuron instance segmentations in MCFO images, neurons can be studied threefold: (1) Clustering and sub-

Table 4. Quantitative results of our baseline models on *combined*, *completely* and *partly* labeled FISBe datasets (continuation of Table 3).

Split	Method	F1 _{0.1}	F1 _{0.2}	F1 _{0.3}	F1 _{0.4}	F1 _{0.5}	F1 _{0.6}	F1 _{0.7}	F1 _{0.8}	F1 _{0.9}
Combined										
Val	ppp	0.62 \pm 0.03	0.57 \pm 0.03	0.53 \pm 0.01	0.50 \pm 0.02	0.49 \pm 0.02	0.43 \pm 0.01	0.28 \pm 0.03	0.22 \pm 0.05	0.10 \pm 0.02
	FFN	0.38 \pm 0.01	0.36 \pm 0.01	0.34 \pm 0.01	0.32 \pm 0.00	0.30 \pm 0.01	0.27 \pm 0.01	0.22 \pm 0.02	0.17 \pm 0.01	0.07 \pm 0.01
	FFN+partly	0.40 \pm 0.02	0.38 \pm 0.02	0.37 \pm 0.02	0.35 \pm 0.01	0.34 \pm 0.01	0.31 \pm 0.01	0.24 \pm 0.01	0.18 \pm 0.01	0.07 \pm 0.01
	Duan et al.	0.38	0.37	0.34	0.33	0.33	0.27	0.18	0.09	0.03
Test	ppp	0.50 \pm 0.01	0.48 \pm 0.01	0.44 \pm 0.01	0.41 \pm 0.02	0.35 \pm 0.02	0.29 \pm 0.02	0.26 \pm 0.01	0.19 \pm 0.02	0.12 \pm 0.01
	FFN	0.34 \pm 0.05	0.31 \pm 0.04	0.28 \pm 0.04	0.25 \pm 0.05	0.22 \pm 0.04	0.20 \pm 0.04	0.17 \pm 0.03	0.12 \pm 0.01	0.07 \pm 0.01
	FFN+partly	0.36 \pm 0.02	0.32 \pm 0.02	0.30 \pm 0.02	0.27 \pm 0.03	0.25 \pm 0.03	0.21 \pm 0.03	0.18 \pm 0.02	0.15 \pm 0.02	0.09 \pm 0.01
	Duan et al.	0.43	0.38	0.35	0.33	0.31	0.29	0.20	0.12	0.06
Completely										
Val	ppp	0.57 \pm 0.07	0.50 \pm 0.05	0.46 \pm 0.02	0.43 \pm 0.05	0.41 \pm 0.07	0.34 \pm 0.03	0.19 \pm 0.02	0.14 \pm 0.07	0.04 \pm 0.02
	FFN	0.31 \pm 0.04	0.28 \pm 0.04	0.26 \pm 0.03	0.24 \pm 0.01	0.24 \pm 0.01	0.22 \pm 0.03	0.16 \pm 0.03	0.13 \pm 0.01	0.04 \pm 0.03
	FFN+partly	0.32 \pm 0.03	0.30 \pm 0.01	0.28 \pm 0.02	0.26 \pm 0.04	0.26 \pm 0.04	0.24 \pm 0.03	0.23 \pm 0.02	0.15 \pm 0.02	0.08 \pm 0.03
	Duan et al.	0.24	0.24	0.24	0.24	0.24	0.20	0.10	0.00	0.00
Test	ppp	0.40 \pm 0.04	0.38 \pm 0.03	0.37 \pm 0.03	0.34 \pm 0.05	0.30 \pm 0.04	0.27 \pm 0.06	0.23 \pm 0.05	0.18 \pm 0.04	0.11 \pm 0.01
	FFN	0.16 \pm 0.11	0.16 \pm 0.11	0.15 \pm 0.10	0.14 \pm 0.10	0.12 \pm 0.08	0.09 \pm 0.06	0.08 \pm 0.05	0.05 \pm 0.04	0.02 \pm 0.02
	FFN+partly	0.15 \pm 0.04	0.15 \pm 0.04	0.14 \pm 0.04	0.12 \pm 0.04	0.11 \pm 0.04	0.10 \pm 0.03	0.08 \pm 0.02	0.07 \pm 0.03	0.03 \pm 0.01
	Duan et al.	0.31	0.29	0.27	0.27	0.27	0.27	0.20	0.14	0.06
Partly										
Val	ppp	0.73 \pm 0.01	0.68 \pm 0.01	0.65 \pm 0.01	0.61 \pm 0.01	0.59 \pm 0.00	0.54 \pm 0.02	0.41 \pm 0.03	0.28 \pm 0.00	0.19 \pm 0.01
	FFN	0.49 \pm 0.01	0.47 \pm 0.01	0.45 \pm 0.02	0.41 \pm 0.01	0.40 \pm 0.01	0.37 \pm 0.01	0.29 \pm 0.03	0.22 \pm 0.02	0.10 \pm 0.02
	FFN+partly	0.50 \pm 0.04	0.47 \pm 0.04	0.46 \pm 0.05	0.42 \pm 0.05	0.41 \pm 0.06	0.36 \pm 0.05	0.26 \pm 0.02	0.22 \pm 0.00	0.09 \pm 0.02
	Duan et al.	0.51	0.49	0.44	0.42	0.42	0.34	0.25	0.18	0.06
Test	ppp	0.62 \pm 0.02	0.58 \pm 0.01	0.51 \pm 0.01	0.47 \pm 0.00	0.40 \pm 0.01	0.33 \pm 0.01	0.28 \pm 0.01	0.21 \pm 0.02	0.17 \pm 0.01
	FFN	0.55 \pm 0.04	0.49 \pm 0.01	0.44 \pm 0.02	0.40 \pm 0.02	0.36 \pm 0.02	0.32 \pm 0.03	0.27 \pm 0.02	0.21 \pm 0.01	0.11 \pm 0.01
	FFN+partly	0.57 \pm 0.06	0.51 \pm 0.04	0.47 \pm 0.03	0.40 \pm 0.04	0.36 \pm 0.03	0.31 \pm 0.03	0.28 \pm 0.03	0.23 \pm 0.02	0.14 \pm 0.02
	Duan et al.	0.55	0.48	0.43	0.39	0.35	0.31	0.19	0.09	0.06

sequent statistical analysis of neuron morphologies may yield insights into neuronal cell types and their variability [15, 19]. (2) Locating a neuron morphology of interest in multiple MCFO images facilitates the creation of novel transgenic lines that sparsely express the neuron of interest, which in turn facilitates functional analyses of individual neurons of interest in vivo [58]. (3) Information on neuron connectivity and neuron function can be fused by locating neurons segmented from electron microscopy (EM) data in MCFO images and subsequent in vivo studies as in (2) [51, 52, 71]. For these tasks, instance segmentations do not necessarily need to cover all true neurons: Given that

MCFO images express only a random subset of neurons in the first place, missing some dim neurons in an instance segmentation, while further reducing recall, does not introduce a categorically new source of error. More specifically, segmenting a subset of neurons with high individual cIDice score is preferable to segmenting all neurons but only partly. We acknowledge these application-derived preferences in our selection of metrics (see Sec. 3 of the main paper).

A.5. Sample Information and Visualization

Table 5 provides a list of the included MCFO acquisitions in the completely labeled FISBe dataset including informa-

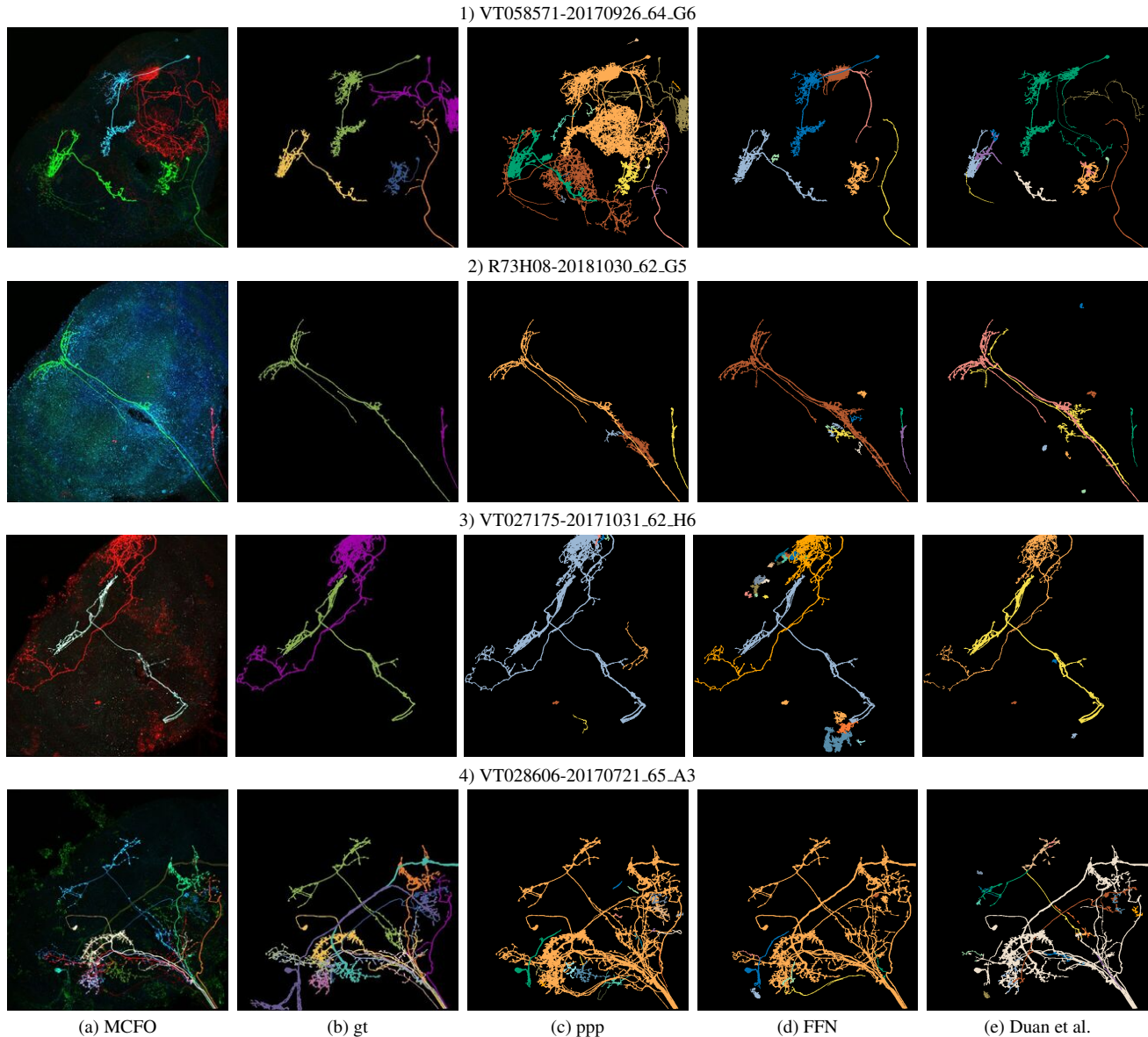


Figure 7. Qualitative results for our three baseline methods: PatchPerPix (ppp), Flood Filling Networks (FFN) and Duan et al.’s color clustering. The columns depict the following: (a): Maximum intensity projection of MCFO sample, (b): ground truth segmentation, (c): ppp prediction, (d): FFN prediction, and (e): Duan et al.’s result. In (1) all three methods yield some correctly segmented neurons, but ppp merges the blue one and one of the red ones, FFN does not segment most of the red ones and Duan et al.’s merges the blue neuron with parts of the red ones; FFN and Duan et al.’s have lower coverage. In (2) the noisy blue channel leads to false positives. In (3) ppp merges the two neurons whereas FFN and Duan et al.’s split them correctly; FFN additionally segments some noise. In (4) all three methods merge multiple neurons of different color; Duan et al.’s has lower coverage.

tion on the split (train/val/test) in which each sample was used. Table 6 provides a list of the included MCFO acquisitions in the partly labeled FISBe dataset including information on the split (train/val/test) in which each sample was used. Fig. 9 shows orthographic view for an exemplary sample. It highlights the thin structures and overall sparseness of foreground. Fig. 10 shows maximum inten-

sity projections together with the gt instance segmentation of all samples in the completely labeled set, separated by train/val/test. Fig. 12 shows maximum intensity projections together with the gt instance segmentation of all samples in the partly labeled set, separated by train/val/test.

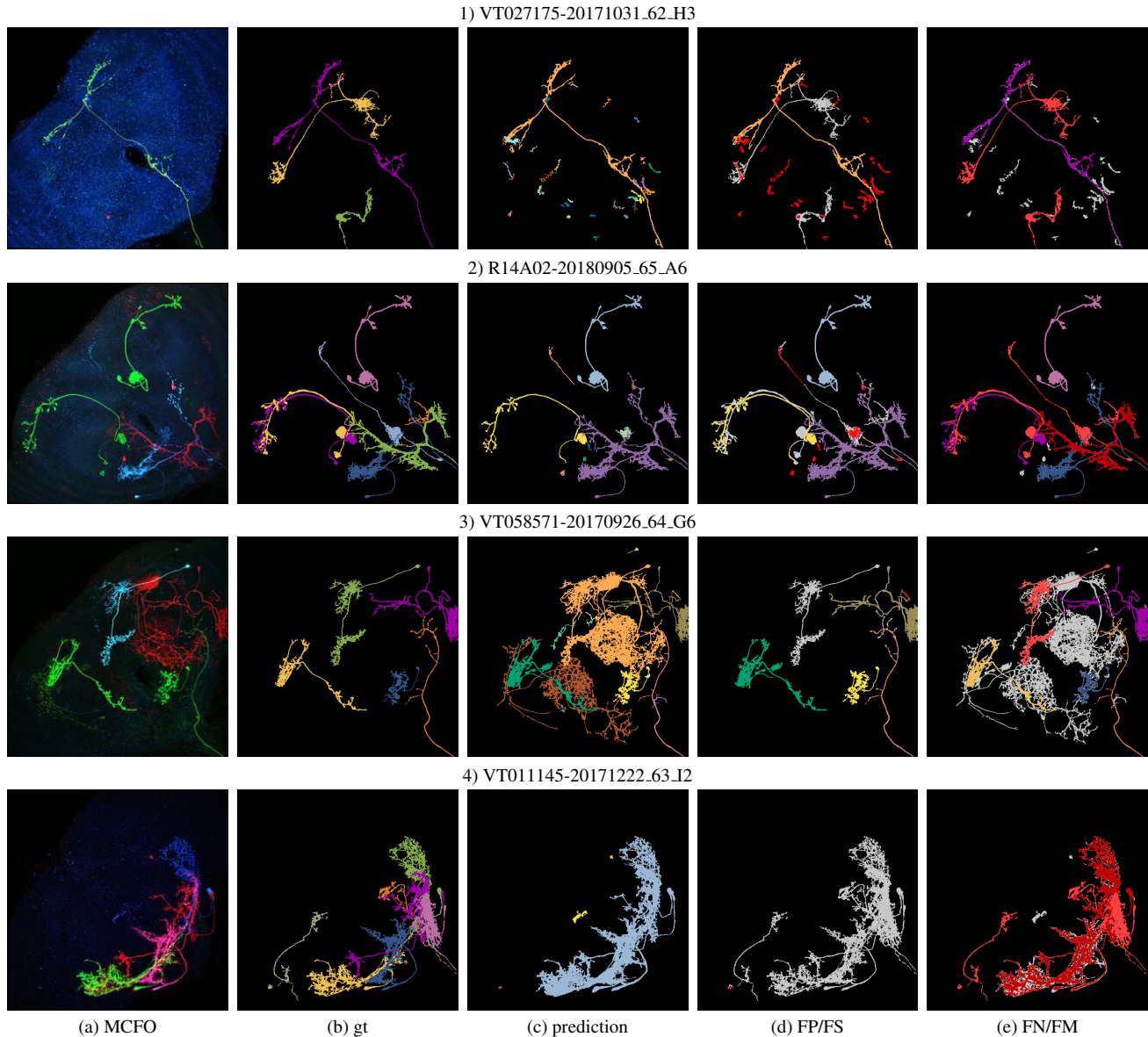


Figure 8. Visualization of the results of our PatchPerPix baseline model for four samples of our completely labeled test set, ground truth-prediction matches are shown for a cIDice threshold of 0.5. ((a): Maximum intensity projection of MCFO sample; (b): ground truth segmentation; (c): predicted segmentation; (d): TP predicted instances in same color code as in (c), FP and FS in red, ground truth in grey; (e): TP ground truth instances in same color code as in (b), FN in light red, FM in dark red, prediction mask in grey.) In (1) the bright green neuron is nicely segmented (see (c), in orange). However, there are two more, very dim neurons in the image, these were missed (see (e) in red). In addition, there is a large number of FP (see (d) in red). In (2) the bright green ones are again nicely segmented (see (c), in yellow and light blue). The purple prediction (see (c)) covers most of the blue and the red neurons, unfortunately resulting in a false merge (FM), despite having very different colors. The blue one still counts as a TP, the red one though as a FN, more precisely a FM (shown in dark red in (e)). There is a very dim red neuron next to the left green one that is missed completely (shown in bright red in (e)). There is a dim blue neuron between the two green ones that is mostly missed resulting in a few FS (shown in red in (d)). In (3) there are a number of unlabeled neurons. There are two bright red neurons, only one is labeled (shown by the absence of a label in (b)). There are a couple of somewhat dim neurons of different colors (there are still visible relatively well when zooming in). We can see that our prediction, as desired, includes the unlabeled neurons (see (c)). We can also see that, as they are not shown in (d) and again as desired, they are counted neither as TP nor as FP. There are again some FM, the bright blue neuron is segmented well but unfortunately the prediction is merged with other neurons (note that it is not shown in dark red (FM) in (e) as it is merged with unlabeled neurons, thus it is not possible to automatically tag it as a FM). (4) shows an extreme FM case. There is a cluster of multiple overlapping bright neurons in different colors (see (a) and (b)). In the prediction they are all merged (shown in dark red in (e)), thus there is no TP (shown by the absence of colored segmentation masks in (d)). In addition there are a number of dim neurons that have been overlooked by the model (shown in bright red in (e)).

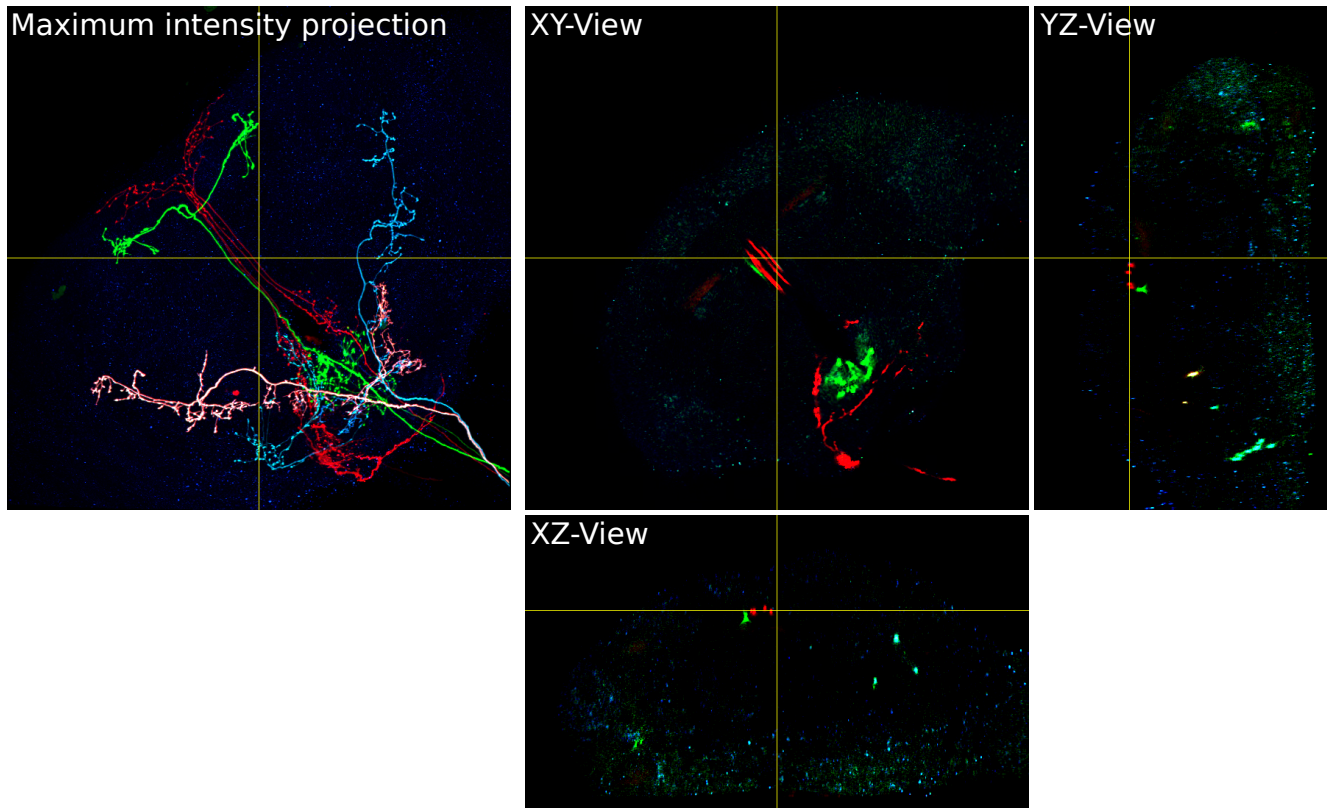


Figure 9. Maximum intensity projection and orthographic views for sample VT007080-20170517.61.A2. The orthographic views highlight the overall sparseness of the foreground and thinness of the neuronal structures.

Table 5. List of MCFO acquisitions in completely labeled FlyLight Instance Segmentation dataset with sample name (<GALA line>-<slide code>), number of annotated neurons, density category and split.

Sample name	Neurons	Cat.	Split	Sample name	Neurons	Cat.	Split
R38F04-20181005.63_G3	2	2	train	VT047848-20171020.66_J2	5	2	train
R38F04-20181005.63_G5	3	2	train	VT047848-20171020.66_I5	12	2	train
R38F04-20181005.63_H1	3	2	train	VT061467-20180911.62_E5	4	2	train
R53A10-20181019.64_A4	1	2	train	R22C03-20180918.66_J2	2	2	val
R75E01-20181030.64_D1	3	2	train	VT012403-20171128.61_B2	5	2	val
VT008647-20171222.63_D2	6	3	train	VT033614-20171124.64_H5	3	3	val
VT008647-20171222.63_D1	7	3	train	VT033614-20171124.64_H1	4	3	val
VT008647-20171222.63_E1	8	3	train	VT041298-20171114.63_C3	7	2	val
VT019303-20171013.65_B6	3	2	train	JRC_SS04989-20160318.24_A2	3	2	test
VT019307-20171013.65_F1	6	3	train	R14A02-20180905.65_A6	7	3	test
VT033051-20171128.61_E4	2	2	train	R54A09-20181019.64_H1	1	2	test
VT033051-20171128.61_E2	4	2	train	VT011145-20171222.63_I1	9	3	test
VT040433-20170919.63_D6	8	2	train	VT027175-20171031.62_H3	3	2	test
VT047848-20171020.66_I3	3	2	train	VT027175-20171031.62_H4	6	2	test
VT047848-20171020.66_I2	4	2	train	VT050157-20171110.61_C1	5	2	test

Table 6. List of MCFO acquisitions in partly labeled FlyLight Instance Segmentation dataset with sample name (<GAL4 line>-<slide code>), number of annotated neurons, density category and split.

Sample name	Neurons	Cat.	Split	Sample name	Neurons	Cat.	Split
R14B11-20180905_65_D2	5	2	train	VT050217-20171110_61_D6	5	2	train
R14B11-20180905_65_D6	9	2	train	VT050217-20171110_61_E1	6	2	train
R24D12-20180921_65_J6	5	3	train	VT058568-20170926_64_E1	13	3	train
R38F04-20181005_63_G2	1	2	train	VT060731-20170517_63_F1	6	2	train
R38F04-20181005_63_G4	2	2	train	VT060731-20170517_63_F2	7	2	train
VT003236-20170602_62_G4	6	3	train	VT061467-20180911_62_E4	1	2	train
VT003236-20170602_62_G5	6	3	train	VT062059-20170727_61_D4	6	2	train
VT007080-20170517_61_A2	4	2	train	JRC_SS05008-20160318_24_B1	4		val
VT007080-20170517_61_A4	10	2	train	JRC_SS05008-20160318_24_B2	6		val
VT007080-20170517_61_A5	15	2	train	R22C03-20180918_66_J1	3	2	val
VT008135-20171122_61_C2	4	2	train	R9F03-20181030_62_B5	3	2	val
VT008647-20171222_63_D5	6	3	train	VT008194-20171222_63_A3	13	2	val
VT008647-20171222_63_D6	7	3	train	VT008194-20171222_63_A5	17	2	val
VT010264-20171222_63_H2	12	3	train	VT012403-20171128_61_B1	6	2	val
VT010264-20171222_63_H5	19	3	train	VT033614-20171124_64_H4	2	3	val
VT011049-20180918_66_I1	2	1	train	VT039350-20171020_64_A1	11	3	val
VT024641-20170615_62_D2	7	2	train	VT039350-20171020_64_A3	8	3	val
VT024641-20170615_62_D3	4	2	train	VT039350-20171020_64_A6	5	3	val
VT024641-20170615_62_D5	5	2	train	VT059775-20170630_63_D5	7	2	val
VT024641-20170615_62_D6	10	2	train	R54A09-20181019_64_H4	4	2	test
VT024641-20170615_62_E1	4	2	train	R54A09-20181019_64_H6	1	2	test
VT025523-20170915_64_I1	11	2	train	R73H08-20181030_62_G5	2	2	test
VT026776-20171017_62_J1	13	3	train	VT006202-20170511_63_C4	8	2	test
VT033051-20171128_61_E3	1	2	train	VT011145-20171222_63_I2	8	3	test
VT033296-20171010_62_B4	4	2	train	VT021537-20171003_61_C3	5	3	test
VT034391-20171128_61_G2	2	2	train	VT023747-20171017_61_F1	10	2	test
VT038149-20171103_62_F1	6	3	train	VT027175-20171031_62_H6	2	2	test
VT039484-20171020_64_C1	7	3	train	VT028606-20170721_65_A2	14	3	test
VT039484-20171020_64_C2	12	3	train	VT028606-20170721_65_A3	12	3	test
VT040430-20170919_63_C4	3	2	train	VT033453-20170721_65_D2	7	2	test
VT040433-20170919_63_E1	6	2	train	VT033453-20170721_65_D4	7	2	test
VT045568-20171020_66_C5	4	2	train	VT033453-20170721_65_D5	5	2	test
VT045568-20171020_66_D2	3	2	train	VT046838-20170922_62_A2	8	2	test
VT047848-20171020_66_I1	6	2	train	VT050157-20171110_61_C5	3	2	test
VT047848-20171020_66_I4	8	2	train	VT058571-20170926_64_G6	5	2	test
VT047848-20171020_66_J1	8	2	train				

Training set

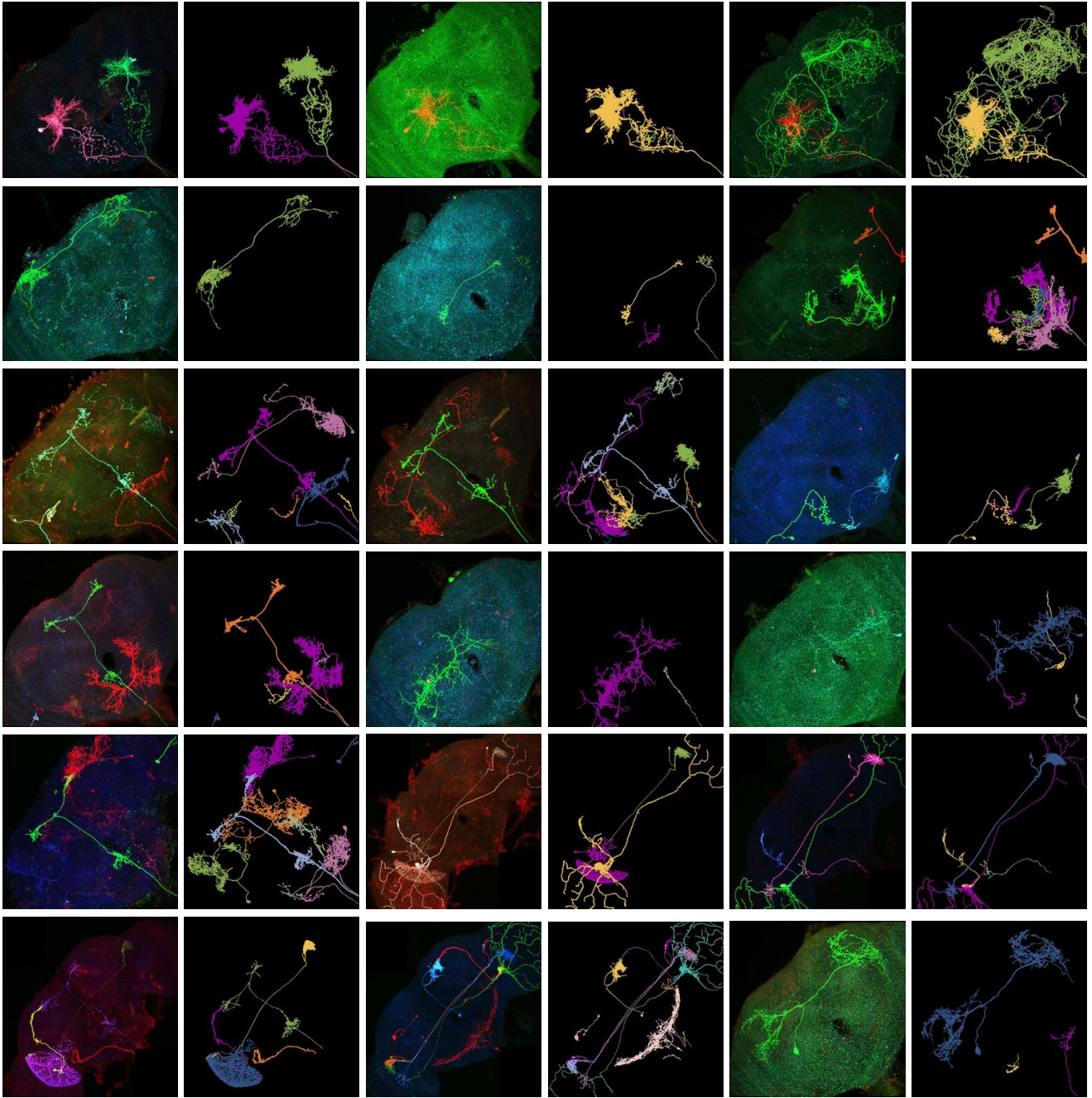


Figure 10. Maximum intensity projections (MIP) of 3d light microscopy samples and ground truth (gt) instance segmentations of all samples in the completely labeled set. MIP and gt are depicted next to each other in alternating order. Images are scaled to same width, some images are center cropped. Figure continued on next page.

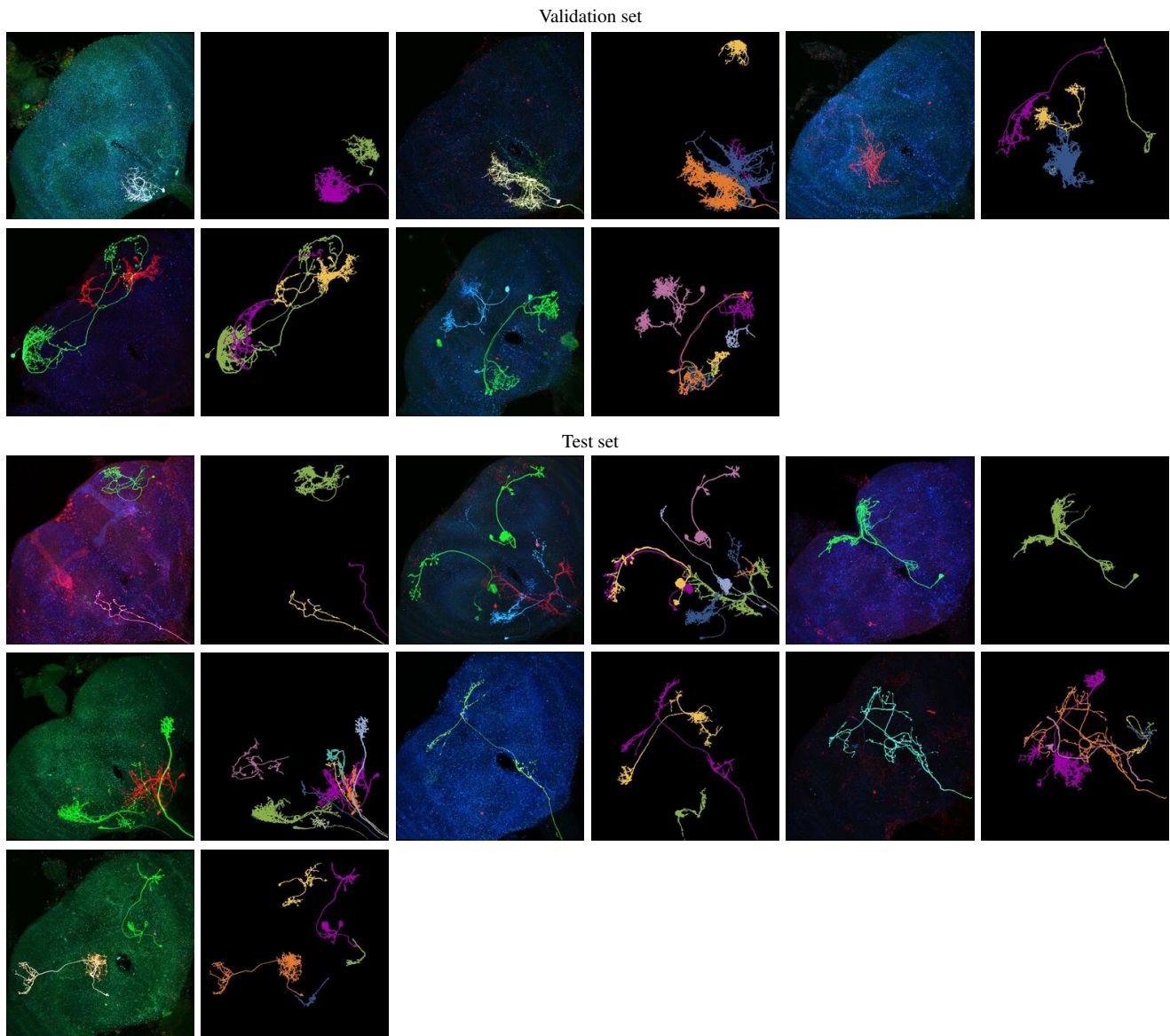


Figure 11. Maximum intensity projections (MIP) of 3d light microscopy samples and ground truth (gt) instance segmentations of all samples in the completely labeled set. MIP and gt are depicted next to each other in alternating order. Images are scaled to same width, some images are center cropped. Figure continued from previous page.

Training set

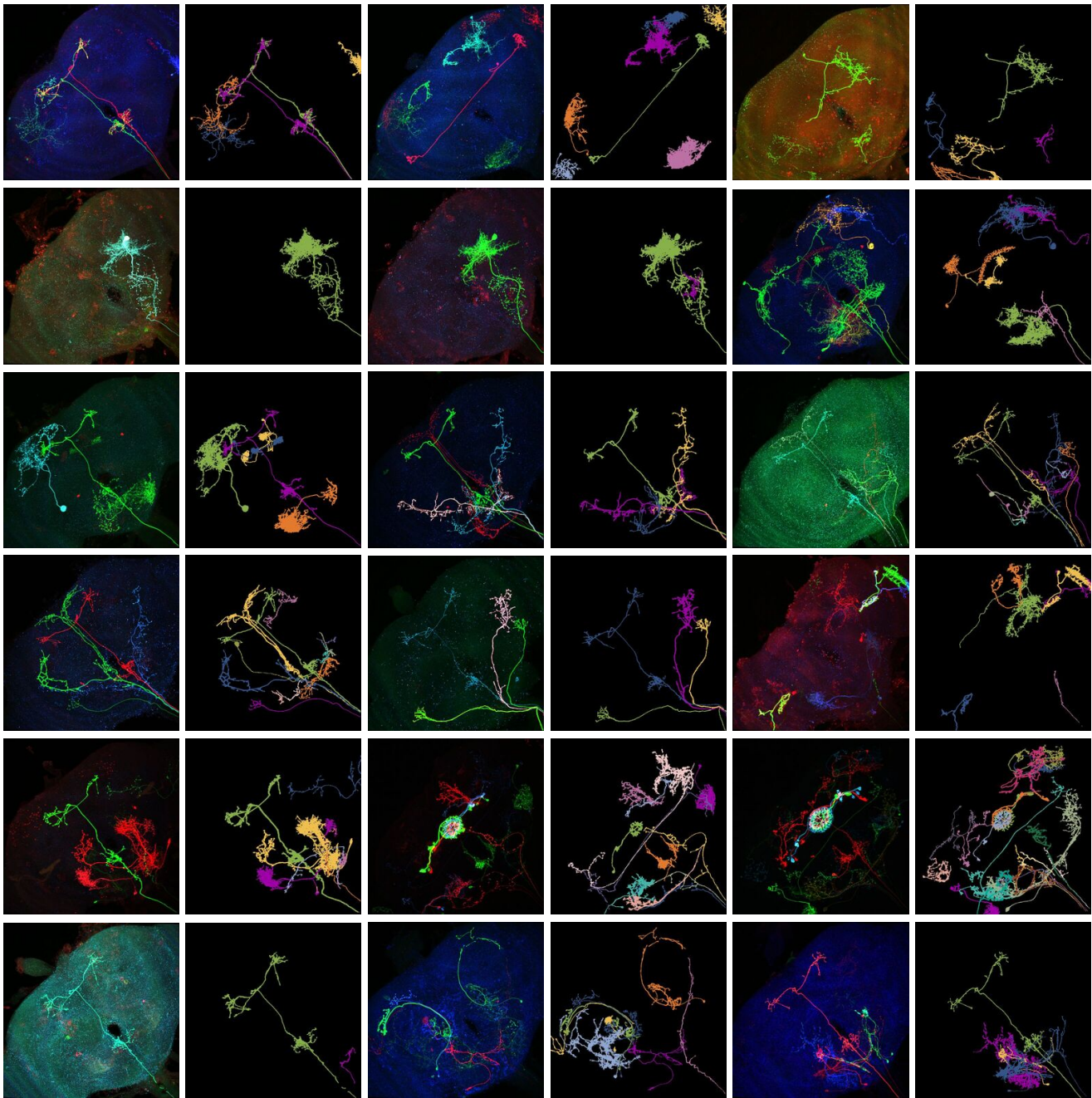


Figure 12. Maximum intensity projections (MIP) of 3d light microscopy samples and ground truth (gt) instance segmentations of all samples in the partly labeled set. MIP and gt are depicted next to each other in alternating order. Images are scaled to same width, some images are center cropped. Figure continued on next page.

Training set (continued from previous page)

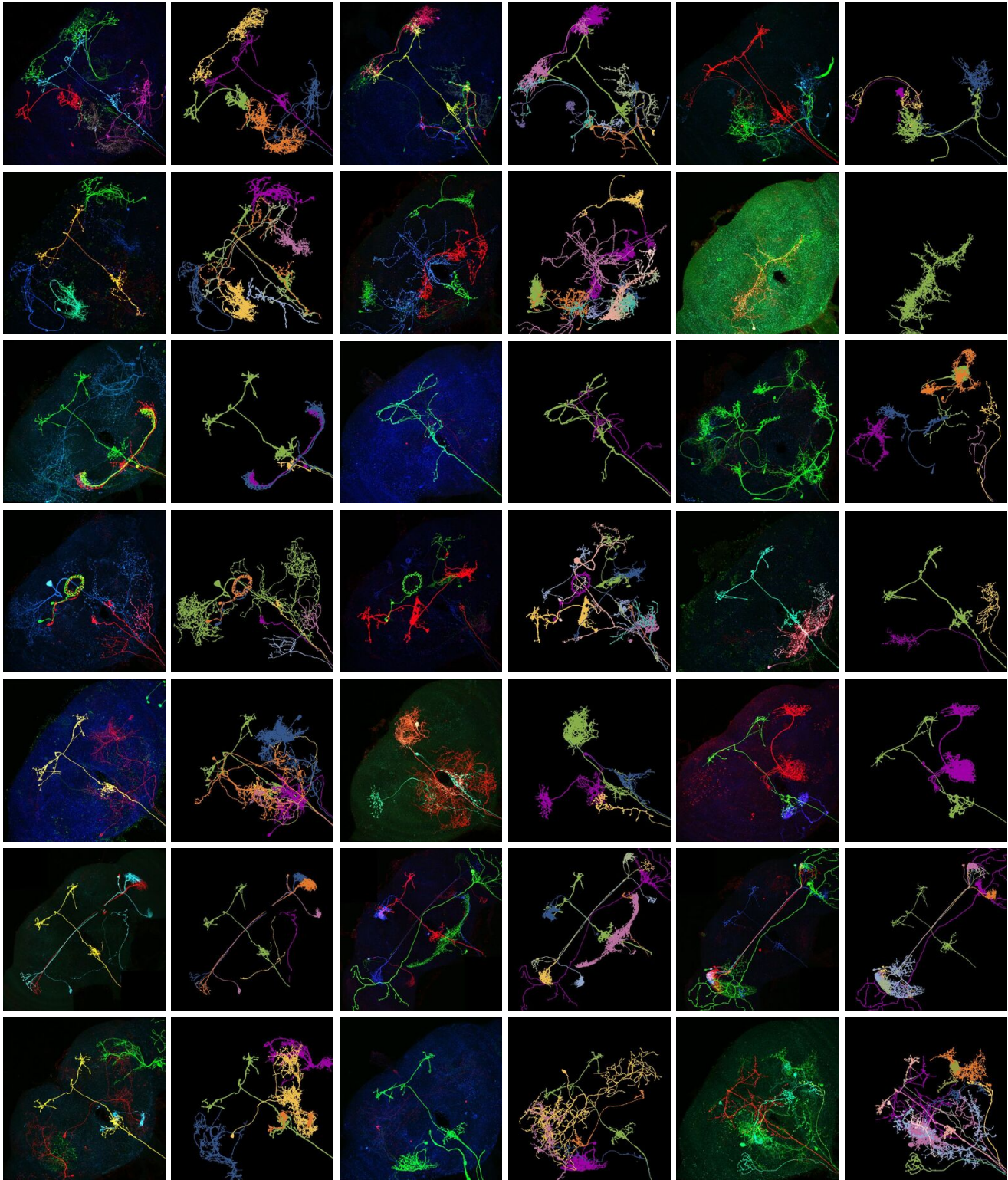
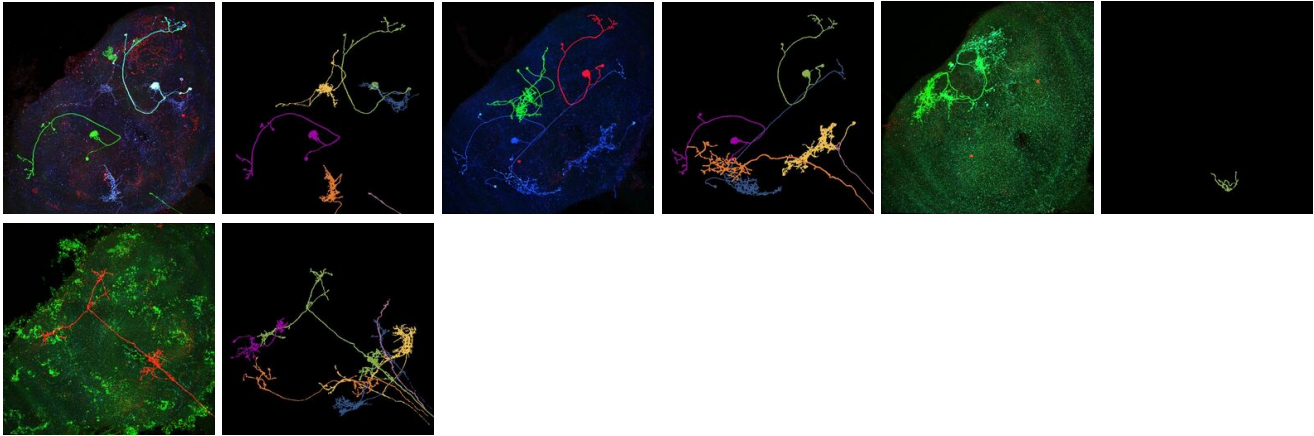


Figure 13. Maximum intensity projections (MIP) of 3d light microscopy samples and ground truth (gt) instance segmentations of all samples in the partly labeled set. MIP and gt are depicted next to each other in alternating order. Images are scaled to same width, some images are center cropped. Figure continued on next page.

Training set (continued from previous page)



Validation set

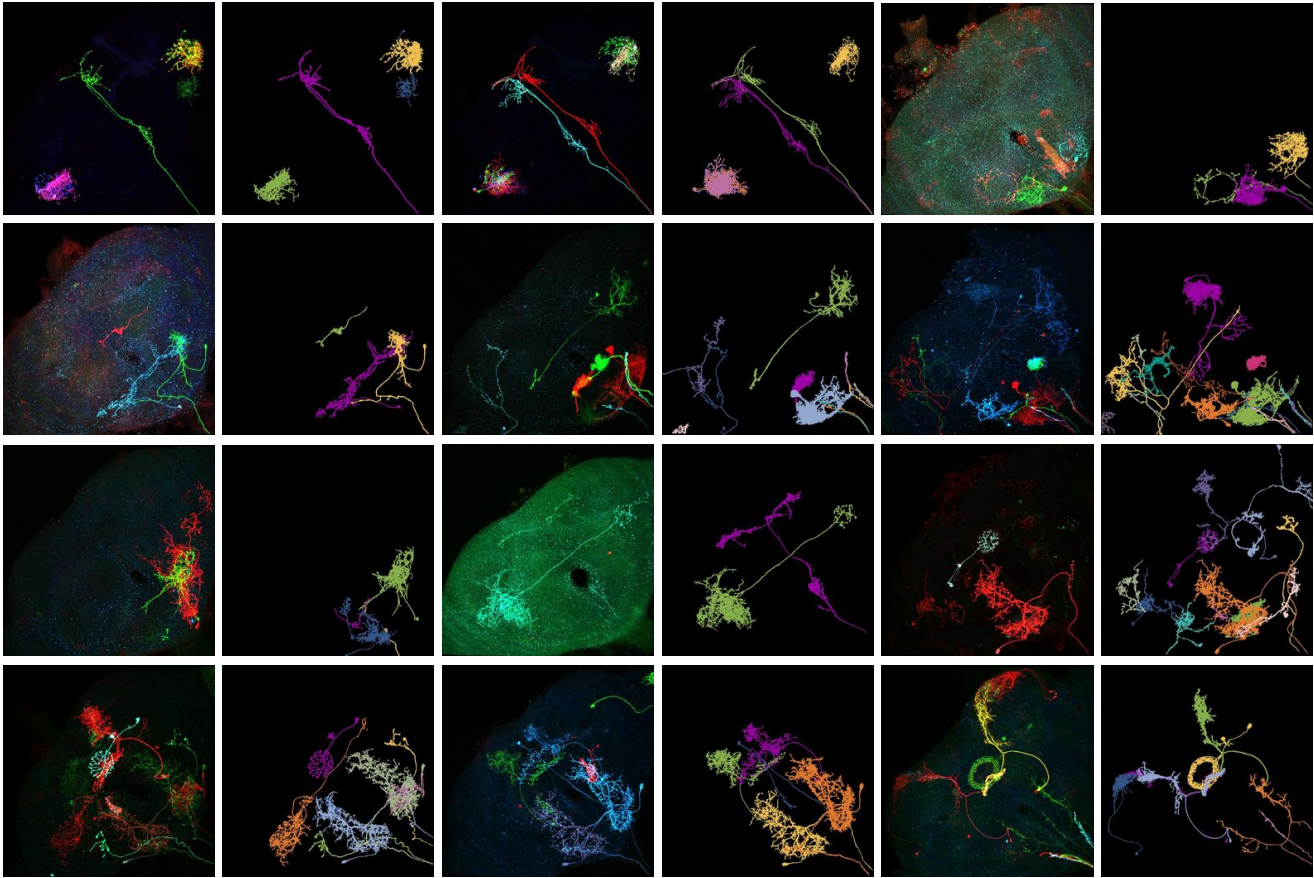


Figure 14. Maximum intensity projections (MIP) of 3d light microscopy samples and ground truth (gt) instance segmentations of all samples in the partly labeled set. MIP and gt are depicted next to each other in alternating order. Images are scaled to same width, some images are center cropped. Figure continued on next page.

Test set

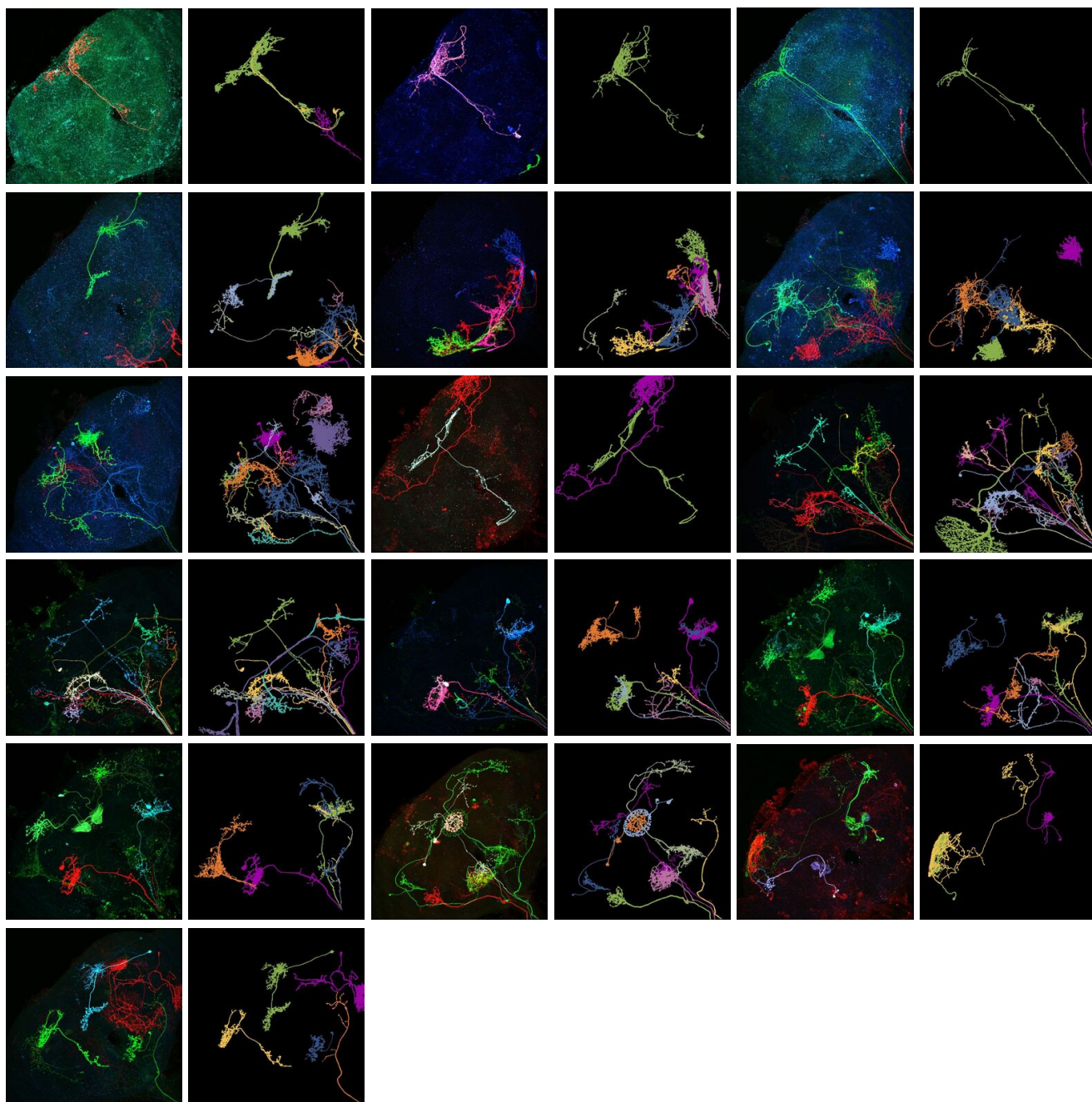


Figure 15. Maximum intensity projections (MIP) of 3d light microscopy samples and ground truth (gt) instance segmentations of all samples in the partly labeled set. MIP and gt are depicted next to each other in alternating order. Images are scaled to same width, some images are center cropped. Figure continued from previous page.